DEVELOPMENT OF WATER GAS SHIFT CATALYSTS FOR CONVERTING SYNTHESIS GAS TO HYDROGEN RICH GAS

MS. EUMPORN BUAROD
ID: 55300700605

A THESIS SUBMITTED AS A PART OF THE REQUIREMENTS
FOR THE DEGREE OF MASTER OF SCIENCE
IN ENERGY TECHNOLOGY AND MANAGEMENT

THE JOINT GRADUATE SCHOOL OF ENERGY AND ENVIRONMENT
AT KING MONGKUT'S UNIVERSITY OF TECHNOLOGY THONBURI

2ND SEMESTER 2013

Development of Water Gas Shift Catalysts for Converting Synthesis Gas to Hydrogen Rich Gas

Ms. Eumporn Buarod
ID: 55300700605

A Thesis Submitted as a Part of the Requirements
for the Degree of Master of Science
in Energy Technology and Management

The Joint Graduate School of Energy and Environment
at King Mongkut's University of Technology Thonburi

2nd Semester 2013

Thesis Committee

………………………………………………	
(Assoc. Prof. Dr. Navadol Laosiripojana)	Advisor
………………………………………………	
(Dr. Sumittra Charojrochkul)	Co-advisor
………………………………………………	
(Dr. Pimpa Limthongkul)	Member
………………………………………………	
(Asst. Prof. Dr. Pisanu Toochinda)	Member
………………………………………………	
(Prof. Dr. Suttichai Assabumrungrat)	External Examiner

Thesis Title: Development of Water Gas Shift (WGS) Catalysts for Converting Synthesis Gas to Hydrogen Rich Gas

Student's name, organization and telephone/fax numbers/email

Miss Eumporn Buarod
The Joint Graduate School of Energy and Environment (JGSEE)
King Mongkut's University of Technology Thonburi (KMUTT)
126 Pracha Uthit Rd., Bangmod, Tungkru, Bangkok 10140 Thailand
Telephone: 0-8518-87051
Email: buaban_47@hotmail.com

Supervisor's name, organization and telephone/fax numbers/email

Assoc. Prof. Dr. Navadol Laosiripojana
The Joint Graduate School of Energy and Environment (JGSEE)
King Mongkut's University of Technology Thonburi (KMUTT)
126 Pracha Uthit Rd., Bangmod, Tungkru, Bangkok 10140 Thailand
Telephone: 0-2872-9014 or 02-470-8309-10 ext. 4146
Email: navadol_l@jgsee.kmutt.ac.th

Co-advisor's name, organization and telephone/fax numbers/email

Dr. Sumittra Charojrochkul
National Metal and Materials Technology Center (MTEC)
114 Thailand Science Park Paholyothin Rd., Klong 1, Klong Luang, Pathumthani 12120
Telephone: 0-2564-6500 ext. 4227, 4118
Email: sumittrc@mtec.or.th

Topic: Development of Water Gas Shift Catalysts For Converting Synthesis Gas to Hydrogen Rich Gas
Name of student: Ms. Eumporn Buarod Student ID: 55300700605
Name of supervisor: Assoc. Prof. Dr. Navadol Laosiripojana
Name of co-supervisor: Dr. Sumittra Charojrochkul

ABSTRACT

The water gas shift reaction is generally applied to produce hydrogen from the reaction of carbon monoxide and water. In the present work, the water gas shift reaction over several ceria-based catalysts (i.e. CeO_2, GDC and YDC) was studied. It is noted that two catalyst preparation methods (i.e. precipitation and low temperature preparation) were compared. Furthermore, the effect of Ni impregnation to promote the reaction was also carried out.

From both preparation techniques, the fluorite oxide-type of CeO_2 was observed, according to XRD characterization. The Gd_2O_3 and Y_2O_3 peaks were not found in GDC and YDC patterns indicating that Gd^{3+} and Y^{3+} incorporated into subsurface region of CeO_2 lattice to form solid solution. An addition of Ni did not cause any change in XRD patterns, presuming that Ni was highly dispersed on the surface of the supports. From the water gas shift activity test, it was found that the impregnation of Ni significantly promoted the catalyst activity. Among the catalysts prepared by low temperature method, 5%Ni/20YDC showed the best activity, from which the CO conversion started at the temperature above 250 °C and reached 75% conversion at 350 °C before dropping at higher temperature as it reached the equilibrium condition. In case of catalysts prepared by co-precipitation method, 5%Ni/CeO_2 showed the highest activity, from which the CO conversion reached 92% conversion at 400 °C. The activation energy and reaction orders of H_2, CO and CO_2 of 5%Ni/CeO_2 were predicted by the kinetics study. From the study, the activation energy (E_a) of 5%Ni/CeO_2 was 27 kJ/mol, while the reaction orders of H_2, CO and CO_2 were 0.69, -0.13 and -0.13, respectively. This indicates the weak negative effect of H_2 and CO_2 on the reaction due to the promotion of reverse water gas shift reaction by both compounds.

Keywords: CeO_2; water gas shift reaction; catalyst; low temperature preparation technique

ACKNOWLEDGEMENTS

The author would like to thank to her advisor Assoc. Prof. Dr. Navadol Laosiripojana for his valuable advice, enthusiastic guidance and encouragement throughout my study. Also thanks to my co-advisor Dr.Sumittra Charojrochkul for giving me a chance to do my thesis at MTEC (National Metal and Material Technology Center) and suggestion throughout my work. The author is also gratefully indebted to the members of examination committee, Dr. Pimpa Limthongkul and Asst. Prof. Dr. Pisanu Toochinda for providing useful advice and suggestions. Profound thanks and appreciation are due to Prof. Dr. Suttichai Assabumrangrat for kindly serving as the external examiner and giving the valuable comments on the research work.

Furthermore, thanks to MTEC (National Metal and Materials Technology Center) and JGSEE (The Joint Graduate School of Energy and Environment) for facilities and supporting the chemicals. Sincere thanks to every research and laboratory staffs who have taught the author during her study. And last, thanks my mom and dad who always encourage me during my work.

CONTENTS

CONTENTS (Cont')

LIST OF TABLES

LIST OF FIGURES

LIST OF FIGURES (Cont’)

CHAPTER 1
INTRODUCTION

1.1 Rationale

The fast depletion of fossil fuel reserves and related environmental concerns are reasons for the renewed interest in alternative energy resources. Alternative energy could be classified into minor categories such as solar energy, wind energy, hydropower, and biomass. Each of them has its own advantage, depending on geography and location. Thailand is an agricultural country, which is abundant with biomass. Therefore, biomass is a suitable alternative energy resource for energy and chemical productions in Thailand. In the last few decades, there are several technologies using biomass as raw materials to produce energy and chemicals. Important technologies include gasification, pyrolysis and hydrolysis (Fig. 1.1). Among these technologies, gasification is known to be the promising biomass conversion technologies, from which the main product from biomass gasification is syngas or synthesis gas. Synthesis gas is a gaseous mixture consisting primarily of hydrogen, carbon monoxide and some carbon dioxide, which can be efficiently converted to several useful fuels and chemicals i.e. alkane, methanol and hydrogen rich gas.

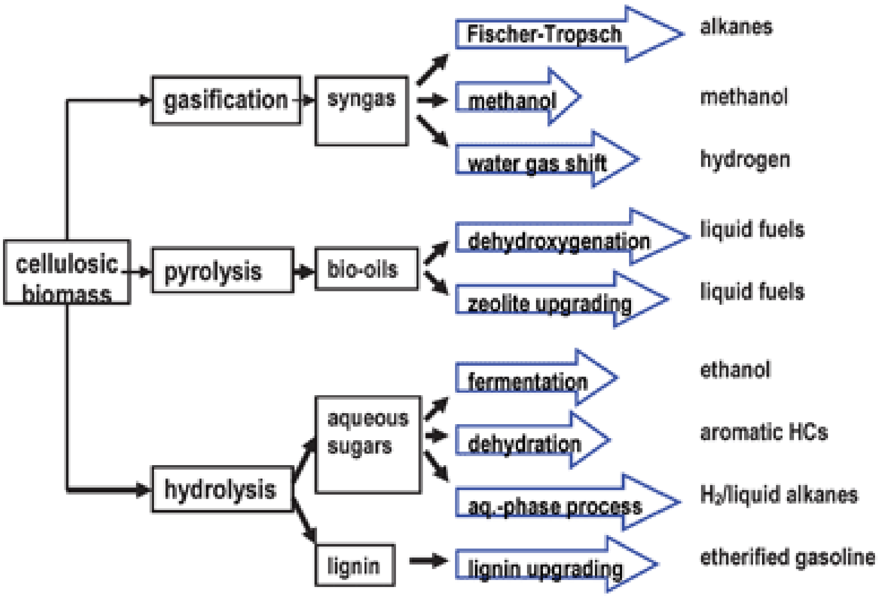

Figure 1.1 Products from renewable resources [1].

In details, synthesis gas is a product from the gasification process of biomass. The process converts fossil based carbonaceous material into carbon monoxide, hydrogen and carbon dioxide by reacting the material at high temperatures (>700°C), without combustion, with a controlled amount of oxygen and/or steam. Currently, synthesis gas is widely used to produce many products, such as hydrogen, methanol, and ethanol (Fig. 1.2). Among these products, hydrogen is a promising fuel for later utilization in a fuel cell.

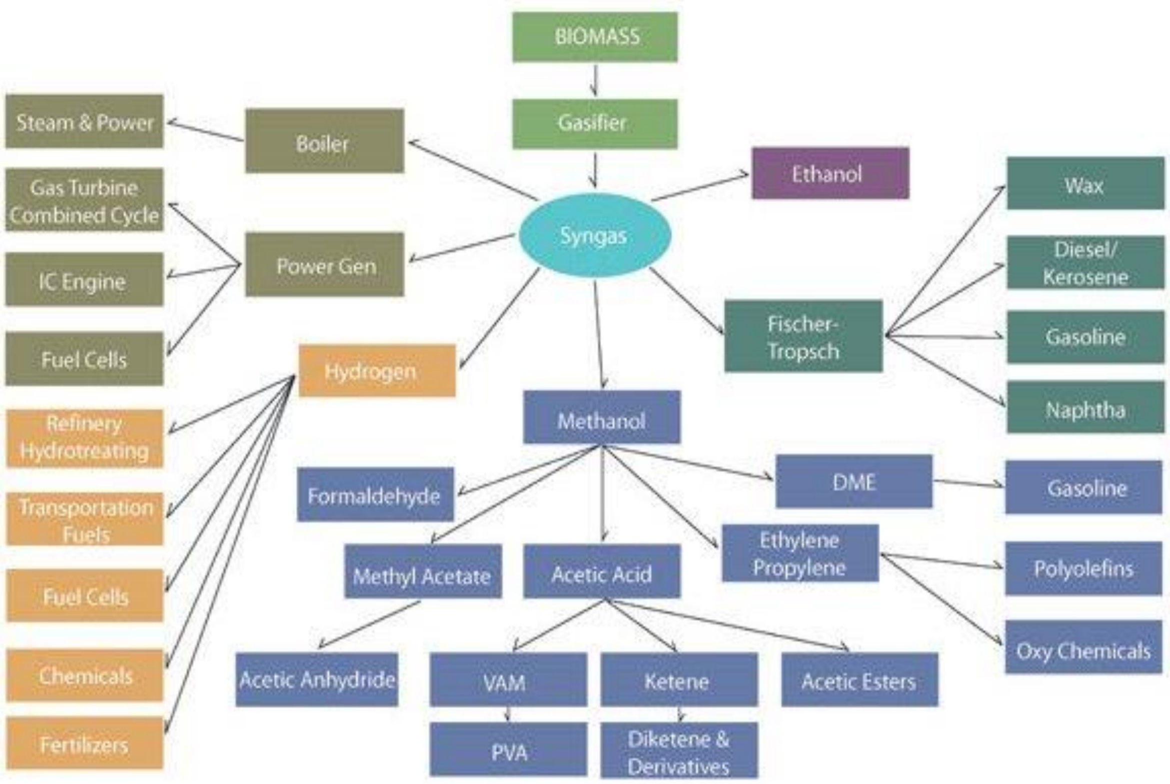

Figure 1.2 Products from the gasification process of biomass [2].

The fuel cell was first demonstrated by Sir William Grove in 1839 [3]. However, its first application was in the early 1960s. The technology is an energy conversion which produces electrical energy and heat with greater energy efficiency and lower pollutant emission than combustion processes [4]. For clean energy production, pure hydrogen is required as a feed gas for electricity generation in fuel cell. Hydrogen is generally produced by steam reforming of hydrocarbons and reformate including a small amount of some gases, such as CO, CO_2, H_2O and CH_4. Among the impurities, CO is poisonous to the Pt electrode in the fuel cell and its concentration must be reduced before entering the fuel cell system.

Until now, the most technologically feasible purification trend is water-gas shift reaction. It was reported to be able to reduce CO from 8% to 1% [5].

$$CH_4 + H_2O \Longleftrightarrow CO + 3H_2 \qquad (1)$$

$$CO + H_2O \Longleftrightarrow CO_2 + H_2 \qquad (2)$$

The water-gas shift reaction (Eq. 2) is always associated with the reforming (Eq. 1) over a catalyst at elevated temperatures. Due to high endothermic reactions, all of these reactions are carried out at high temperature (700-900°C). The WGSR is one of the most important reactions used to balance the H_2/CO ratio. The equilibrium of this reaction shows a significant temperature dependence and the equilibrium constant decreases with an increase in temperature, that is, higher carbon monoxide conversion is observed at lower temperatures. In order to take advantage of both thermodynamics and kinetics of the reaction, the industrial scale water gas shift reaction is conducted in multiple adiabatic stages consisting of a high temperature shift (HTS) followed by a low temperature shift (LTS) with intersystem cooling [6].

The initial HTS takes advantage of the high reaction rates, but is thermodynamically limited, which results in the incomplete conversion of carbon monoxide and a 2-4% carbon monoxide exit composition. To shift the equilibrium toward hydrogen production, a subsequent low temperature shift reactor is employed to produce a carbon monoxide exit composition of less than 1%. The transition from the HTS to the LTS reactors necessitates intersystem cooling. Due to the different reaction conditions, different catalysts must be employed at each stage to ensure optimal activity. The commercial HTS catalyst is the iron oxide–chromium oxide catalyst. The chromium acts to stabilize the iron oxide and prevents sintering. The operation of HTS catalysts occurs within the temperature range of 310°C to 450°C [7]. The commercial LTS catalyst is a copper-based catalyst. The typical composition of commercial LTS catalyst has been reported as 32-33% CuO, 34-53% ZnO, 15-33% Al_2O_3 [3]. The LTS shift reactor operates at a range of 200°C to 250°C [8].

1.2 Research Objectives

- To synthesize GDC and YDC-based catalysts via low temperature and co-precipitation techniques and impregnate Ni to promote the catalytic activity.
- To study the catalytic activity of synthesized catalysts toward the water gas shift reaction
- To optimize the operating conditions of the reaction to maximize the yield of H_2 production by varying temperatures and percentages of CO, H_2 and CO_2 used in water gas shift reaction.

1.3 Scope of research work

- To compare two catalyst preparation methods on yielding the highest amount of Hydrogen rich gas production.
- To study the WGS activity over monometallic (i.e. Ni) supported on CeO_2 and doped ceria (i.e. Gd-CeO_2, Y-CeO_2) between 100-500˚C.
- To investigate activity controlling factors by studying surface area, particle size, morphology of the catalysts and supports using BET surface area, X-ray diffraction (XRD), Scanning electron microscopy (SEM) and Temperature – programmed reduction (TPR).

CHAPTER 2
LITERATURE REVIEW

2.1 Hydrogen rich gas and Fuel cells

Hydrogen is a weight light gas. It is a colorless, highly flammable gaseous element, the lightest of all gases and the most abundant element in the universe. The atomic number of this element is 1.0 and the element symbol is H [9]. At room temperature hydrogen is a gas, but when cooled to very low temperatures (below -253° C) it becomes liquid. In recent years, hydrogen has become a widely used feedstock in a chemical, petroleum refining, and petrochemical industries [10].

Scientists had been producing hydrogen for years before it was recognized as an element. Written records indicate that Robert Boyle produced hydrogen gas as early as 1671 while experimenting with iron and acids. Hydrogen was first recognized as a distinct element by Henry Cavendish in 1766. Hydrogen is a commercially important element. A large amount of hydrogen is combined with nitrogen from air to produce ammonia (NH_3) through a process called Haber process. Hydrogen is also added to fats and oils, such as peanut oil, through a process called hydrogenation. Liquid hydrogen is used in the study of superconductors and, when combined with liquid oxygen, makes an excellent rocket fuel. Hydrogen combines with other elements to form numerous compounds. Some of the common ones are: water (H_2O), ammonia (NH_3), methane (CH_4), table sugar ($C_{12}H_{22}O_{11}$), hydrogen peroxide (H_2O_2) and hydrochloric acid (HCL). Another common use is the manufacture of chemicals with specific end uses, such as for pharmaceuticals; hydrogenation reactions and fuel cell [11].

A fuel cell is an energy conversion unit that converts a gaseous fuel to electrical energy and heat by electrochemical reaction of fuel with an oxidant. Fuel cells produce energy in the form of electricity and heats as long as fuel can be supplied. Since the fuel cell is operated electrochemically and is not limited by the Carnot cycle, lower emission such as NO_x or CO_2 are produced from fuel cells compared to the cleanest combustion process. Because of its high conversion efficiency and environmental acceptability, the fuel cell is regarded as an effective process to produce electricity from chemical components. Moreover, this technology also presents flexibility and modularity, as it does not suffer appreciably from problems of lubrication, wear and heat loss, which affect the reliability of traditional heat engines[12].

A fuel cell normally consists of 3 main sections: anode, cathode and electrolyte. A fuel and an oxidant, supplied from external sources, are introduced to the anode and cathode side. Both could be any gases capable of being electrochemically oxidized and reduced. In detail, fuel (e.g. Hydrogen) is oxidized at the anode side by electrochemical oxidation process producing electrons. Electrons transport along the external circuit and reduce the oxidant (e.g. Oxygen) at the cathode side. Ions from this reduction process then pass through the electrolyte, which conducts only O^{2-} ions to the anode part and H^+ ions to the cathode part in order to complete the electrical circuit. The driving force of the operation is the chemical potential gradient of oxygen across the electrolyte. Direct-current electricity was consequently produced in the external circuit. In the real application, fuel cells are connected in a series of cells in order to obtain higher outlet voltage. An interconnect plate is always installed to provide the electronic contact between the anode of one cell and the cathode of the next cell [12]. Several types of fuel cells have been developed. They are classified according to their different electrolytes and operating temperature. Also different anode and cathode catalyst can be classified as shown in Tables 2.1 and 2.2.

Table 2.1 Main types of fuel cells [13].

Fuel cell type	Abbreviation	Electrolyte	Operating temperature (°C)
- Alkaline	AFC	Potassium hydroxide	50 - 90
- Proton Exchange Membrane	PEMFC	Solid proton conducting polymer	50 - 125
- Phosphoric acid	PAFC	Orthophosphoric acid	190 - 210
- Molten carbonate	MCFC	Lithium/Potassium carbonate mixture	630 - 650
- Solid oxide	SOFC	Stabilised zirconia	700 - 1100
- Direct methanol	DMFC	Sulphuric acid or solid polymer	50 - 120

Table 2.2 Electrocatalysts in fuel cell systems[13].

Fuel cell type	Anode material	Cathode material
- Alkaline (AFC)	Pt/Au, Pt, Ag	Pt/Au, Pt, Ag
- Proton Exchange Membrane (PEMFC)	Pt, Pt/Ru	Pt
- Phosphoric acid (PAFC)	Pt	Pt/Cr/Co, Pt/Ni
- Molten carbonate (MCFC)	Ni, Ni/Cr	Li/NiO
- Solid oxide (SOFC)	Ni/ZrO_2	(LaSr)MnO_3

Alkaline Fuel Cells (AFC) were developed by NASA for the Apollo spaceship module[14]. It was used to produce electrical power supply for the space shuttle orbiters [15]. A major problem of this type of fuel cell is the low tolerance to CO/CO_2 in feed gases for the alkaline electrolyte.

Proton Exchange Membrane Fuel Cells (PEMFC) are believed to be the best fuel cell in the vehicular power source, eventually replacing the gasoline and diesel. Compared to the others, generating more power for a given volume or weight of fuel cell is the great advantage of PEMFC. Moreover, the output of this fuel cell could be varied quickly to meet shift in power demand. Therefore, PEMFC is suitable for the automobile applications, where quick startup is required. According to the U.S. Department of Energy, this type of fuel cell is the primary candidate for light-duty vehicles, for building, and potentially for smaller applications such as replacements of rechargeable batteries [16].

Phosphoric Acid Fuel Cells (PAFC) are the first fuel cells to be commercialized and be the most commercially developed of fuel cells. Many Phosphoric Acid Fuel Cell systems have been installed in diverse applications such as hospitals, nursing homes, hotels, office buildings, schools, utility power plants and airport terminal. Moreover, this fuel cell can also be applied in large vehicles, such as buses and locomotives [16]. PAFC uses phosphoric acid (H_3PO_4) as electrolyte. The ionic conductivity of phosphoric acid is low at low temperature. Phosphoric acid is immobilized in a porous separator matrix consisting of silicon carbide powder bonded with polytetrafluoroethylene (PTFE). The non-reaction of phosphoric acid and carbon dioxide of PAFC when operated in a cogeneration mode is a great advantage. In addition, CO_2 does not affect the electrolyte or cell performance and can therefore be easily operated with reformed fossil fuel. However, carbon monoxide in the fuel gases could degrade the performance of Pt-based anode electrocatalysts.

Molten Carbonate Fuel Cells (MCFC) produce high electricity efficiency as well as have high ability to consume coal-based fuels. Due to its high operating temperature, this allows the use of natural gas directly. The first full-scale molten carbonate stacks were tested and demonstrated in California in 1996. The fuel supplied for this type of fuel cell can be hydrogen, carbon monoxide, natural gas, propane, landfilled gas, marine diesel and simulated coal gasification products [16]. Due to the high operating temperature, these fuels are internally reformed at the anode directly by mixing with steam.

Solid Oxide Fuel Cells (SOFC) are solid-state energy conversion units that appear to be the most promising of the fuel cell systems. This type of fuel cell is the main focus of this work, Solid Oxide Fuel Cell, has been particularly of interest due to its high conversion efficiency and fuel management [17]. Similar to other type of fuel cells, SOFC requires the fuel such as hydrogen, and oxidant such as oxygen or air to electrochemically react at high temperature and generate electrical energy. Hydrogen is normally used as a fuel since it has high electrochemical activity, but, carbon monoxide can also be used as the fuel together with hydrogen. The direct use of a hydrocarbon gas instead of hydrogen or carbon monoxide could lead to the deactivation at fuel cell electrode by carbon deposition. SOFC has several advantages over other types of fuel cells. It is able to convert carbon monoxide as well as hydrogen, and the high operating temperature allows internal reforming of gaseous fuel and promotes rapid kinetics to produce high quality heat energy conversion. The SOFC electrolyte is a solid ceramic membrane. The solid-state electrolyte could reduce corrosion, and eliminate electrolyte management problems.

Direct Methanol Fuel Cells (DMFC) are quite similar to PEMFC. This technology is still in the early stages of development, but it has been successfully demonstrated to power mobile phones in future years. Both of them, DMFC and PEMFC, use polymer membrane as the electrolyte. However, for DMFC, the anode catalyst itself draws the hydrogen from the liquid methanol, eliminating the need for a fuel reformer [16].

2.2 Hydrogen Production Process

The main fuel for this technology is hydrogen. About 93% of all the atoms in the earth are hydrogen. Hydrogen is the most abundant element in the universe. Hydrogen has the problem from hydrogen storage. Therefore hydrogen production has been studied and developed for many years [18, 19]. The main advantages in using hydrogen are health and environment friendly, problem on fossil fuels, superior efficiency and clean renewable energy.

Theoretically, hydrogen can be derived from a host of different hydrocarbons through various techniques. The methods can be classified into three main types based on hydrogen sources including fossil fuel, water and organic compounds (Fig. 2.1) [19].

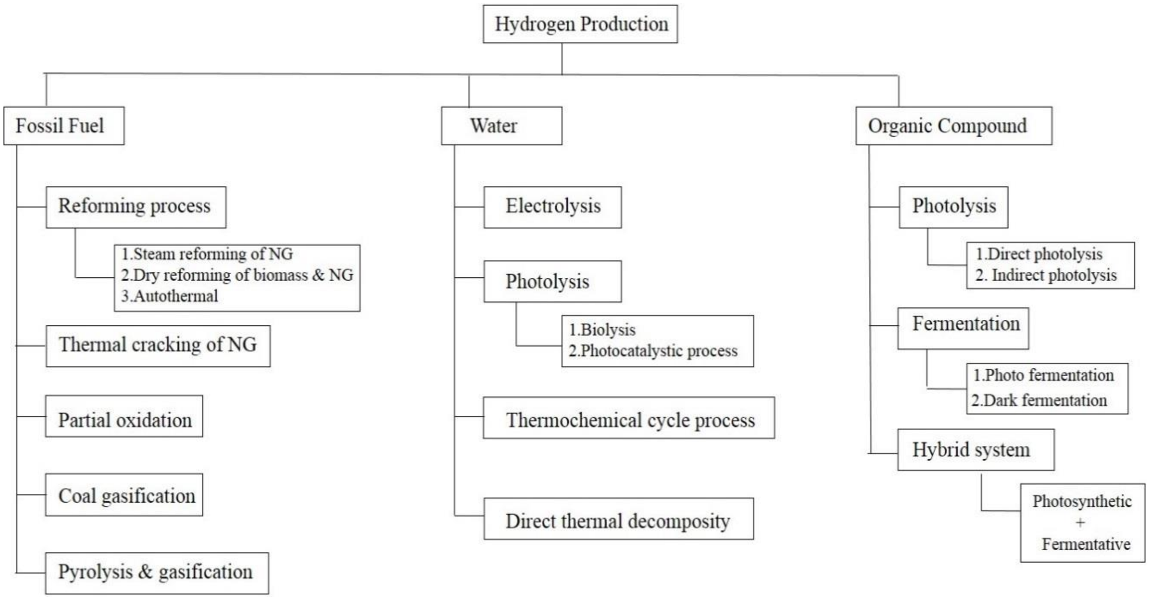

Figure 2.1 The classification of hydrogen production by reactance [14].

For the first approach (i.e. hydrogen production from fossil fuels), many methods have been reported to use the hydrogen production process from fossil fuels, such as gasification, partial oxidation, autothermal reforming, etc. Anyway, the majority of all these processes are based on heating up hydrocarbon, steam and some amount of air or oxygen, which are then combined in a reactor. The water molecule and the raw material, such as natural gas, in this process are splited to release H_2, CO and CO_2. The hydrogen atom, thus, comes from both steam and the hydrocarbon compounds.

Steam reforming reaction $CH_4 + H_2O \Longleftrightarrow CO + 3H_2$ (3)
Partial oxidation reaction $CH_4 + 1/2O_2 \Longleftrightarrow CO + 2H_2$ (4)
Dry reforming reaction $CH_4 + CO_2 \Longleftrightarrow 2CO + 2H_2$ (5)
Autothermal reforming $CH_4 + 1/2H_2O + 1/4O \Longleftrightarrow CO + 5/2H_2$ (6)
Water gas shift reaction $CO + H_2O \Longleftrightarrow CO_2 + H_2$ (7)

One of the most outstanding hydrogen production process is steam reforming, widely used to generate hydrogen for later utilization in fuel cell due to the main advantages such as containing higher H:C ratio than other reactions, H:C = 3:1. Moreover, the product steam from the reaction can be used to enhance the reforming reaction (eq.3) by the water gas shift reaction (eq.7) producing additional hydrogen.

Secondly, hydrogen can be generated from water since hydrogen is 11.2% in water measured by weight, and over 70% of the earth is covered with water. Water is one of the majority and interesting source of the hydrogen. Water is broken down to release hydrogen and oxygen. Although this kind of hydrogen source is environmental friendly, this process required more energy such as heat, electricity, light or chemical energy to break down the chemical bond. For the hydrogen production from organic compound, it is related to the biological process. The main system is photosynthesis to split water into hydrogen and oxygen. Hydrogen from this process is usually created in the form of hydrocarbon by mixed hydrogen with carbon dioxide by chlorophyll catalytic.

Another classification of hydrogen production is by its production process (Fig. 2.2). Hydrogen production can be classified into 3 types, including chemical process, biological process and electrochemical process.

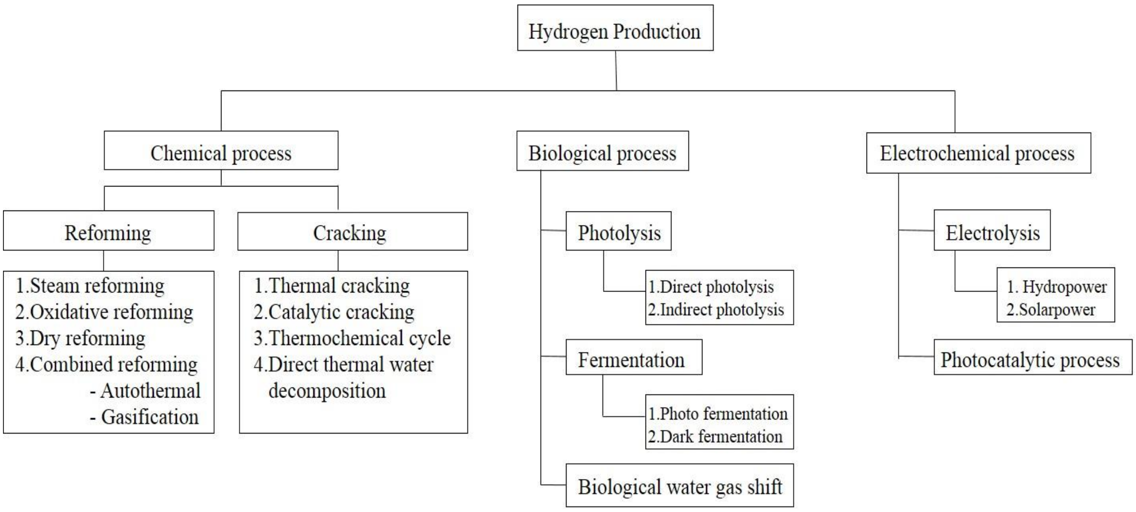

Figure 2.2 The classification of hydrogen production by process.

Due to the large known reserves of natural gas and the need to reduce the use of petroleum as the feeding fuel, intense research of this gas has been done and it is expected to be used as the transportation fuel to replace gasoline and diesel[20]. Methane catalytic steam reforming is a well-established process for converting natural gas into hydrogen as methane is abundant and contains greater H:C ratio among other hydrocarbon [21].

2.3 Reactions related to fuel cell technology and hydrogen production

Fuel cell used as a simple chemical reaction to combine hydrogen and oxygen into water, producing electric current in the process. No pollution is produced via this reaction; the only byproducts from the fuel cell are water and heat. The fuel cell reaction are explained in the reactions below

$$\text{Anode} \quad 2H_2 \longrightarrow 4H^+ + 4e^- \quad (8)$$

$$\text{Cathode} \quad 4e^- + 4H^+ + O_2 \longrightarrow 2H_2O \quad (9)$$

$$\text{Overall} \quad 2H_2 + O_2 \longrightarrow 2H_2O + \text{heat} \quad (10)$$

The ideal fuel for current fuel cells is pure hydrogen. Hydrogen is produced from reforming process in which available fuel such as natural gas, gasoline, propane (LPG), diesel fuel and methanol are used as the input gas.

$$\text{Fuel} \longrightarrow \text{Reforming} \longrightarrow \text{WGS} \longrightarrow \text{PROX} \longrightarrow H_2$$

$$\text{Reforming:} \quad CH_4 + H_2O \longrightarrow CO + 3H_2 \tag{11}$$

$$\text{WGS:} \quad CO + H_2O \longrightarrow CO_2 + H_2 \tag{12}$$

$$\text{PROX:} \quad 2CO + O_2 \longrightarrow 2CO_2 \tag{13}$$

From this process, the major steps are reforming, water gas shift and CO preferential oxidation (PROX). The reforming processes are available for the initial transformation of fuel. The reforming route is generally conducted at high temperature using catalysts to convert the hydrocarbon source to carbon monoxide and hydrogen as a product. The reforming process produces hydrogen rich gas contains 8-12% CO depending on the steam-to-carbon and air-to-fuel ratios in the reformer feed. For use in proton exchange membrane fuel cell, the reformer product must be further processed to reduce the CO concentration to <10 ppm because of the poisoning effect of CO on the Pt-based anode catalyst [22].

Water gas shift (WGS) is an important step in fuel processors for preliminary CO clean up and additional hydrogen generations prior to the final CO clean up stage. The WGS reaction is used to convert carbon monoxide to carbon dioxide and hydrogen through a reaction with water [23]. Finally, preferential oxidation (PROX) is conducted in a clean-up system to convert the remaining CO to < 10-50 ppm[24]. This process can reduce CO to the desired level before feeding into a fuel cell system.

$$CO + H_2O \longrightarrow CO_2 + H_2 \qquad \Delta H^\circ = -41.1 \text{ KJ/mol} \tag{14}$$

$$2CO + O_2 \longrightarrow 2CO_2 \tag{15}$$

2.4 Catalysts

A catalyst is a chemical compound that is capable of directing and accelerating the thermodynamic reaction by reducing the activation energy of a reaction while themselves remaining unaltered at the end of the process [25]. Catalysis is the increase in the rate of a chemical reaction of one or more reactants due to the participation of an additional substance[26]. Unlike other reagents in the chemical reaction, a catalyst is not consumed by the reaction. With a catalyst, less free energy is required to reach the transition state, but the total free energy from reactants to products does not change [26].

2.4.1 Properties and Characteristics of Industrial Catalysts

There are 10 properties of catalysts that should be realized before selecting one of them: activity, selectivity, stability, morphology, mechanical strength, thermal characteristic, regenerability, reproducibility, originality and cost [27]. For activity, each catalyst has their specific activity. Catalyst should also produce high selectivity and yield of desired product through the condition. In the other words, the texture of the catalyst should be improved toward reducing limitations. A good stability catalyst changes very slowly over the course of time and under the using condition. The change or deactivation of catalyst can be from (a) Coke formation: carbon atom from the hydrocarbon compound will encapsulate the catalyst particle and block the reforming ability; (b) Volatile agent such as chlorine, reactants, products and poisons may attack active agents or the support; and (c) The regrouping or enlarging of the crystals deposited by metal. It should also be noted that the external morphological characteristics of a catalyst such as the form and the grain size must be suitable for the corresponding process. Under some operating condition such as the reforming process, when operating with high pressure and high temperature, the mechanical strength and the thermal characteristics should also be considered. The mechanical strength of the catalyst concludes its resistance to crushing which enables the catalyst to pass undamaged through all the strains. While the thermal characteristic consisting of thermal conductivity and specific heat requires consideration.

As described, the catalyst can be deactivated by the above factors. The regenerability of the catalyst, thus, is needed and this relates to the stability. When the catalysts have become insufficient, they must be regenerated through a treatment that will return part or all of their catalytic properties.

2.4.2 Types of catalyst

There are many methods to classify catalysts. For example: classifying by the different preparation processes. Regarding this, there are 2 types of catalyst: bulk catalysts and the supported catalysts [28]. Another classifying is by phase and the reaction medium, for this, there are 2 types of catalyst. The first is the homogeneous which it has the same phase or can be dissolved in the reaction medium [25]. Second is the heterogeneous, the properties of it can change significantly with use and/or with operation condition that vary from minuets to years [28]. A typical heterogeneous catalyst consist mainly of 3 components: (1) an active catalyst, (2) a support which helps increasing the active catalyst dispersion and reducing the active catalyst sintering and (3) a catalyst promoter.

2.5 Catalysts for water gas shift reaction

Since the water gas shift reaction is an exothermic reaction, it is favored at low temperatures. The current water gas shift catalysts are kinetically limited at low temperatures since they are not active enough to attain equilibrium. Current commercial large-scale industrial plants often use two-step process employing high temperature shift catalyst and low temperature shift catalyst [54]. Iron oxide – chromium oxide catalyst were developed for high temperature catalyst. It can be operated in the temperature range of 310°C to 450°C and are called ferrochrome catalysts because of their composition. Copper based catalyst was developed to be operated at lower temperature in the range of 200°C to 250°C [55]. Cerium (IV) oxide, also known as ceria, cerium oxide or cerium dioxide, is an oxide of the rare earth metal cerium. It is a pale yellow-white powder with the chemical formula CeO_2. Cerium (IV) oxide is formed by the calcination of cerium oxalate or cerium hydroxide. CeO_2 has the fluorite type crystal structure with space group Fm3m (Fig. 2.3). Cerium oxide is highly promising support for water gas shift catalysts because of its ability to undergo rapid reduction and oxidation cycle [56, 57]. Ceria can also serve as a stabilizer for alumina and other metal oxide supports, maintaining a high dispersion of the catalyst component [58]. The association of other rare earth element into ceria is reported to improve the structural stability of ceria toward sintering and also enhance water gas shift activity [59]. Rare earth oxide dopants such as Y_2O_3 and Gd_2O_3 form solid solution with ceria and demonstrate a significant improvement in electrical properties [36].

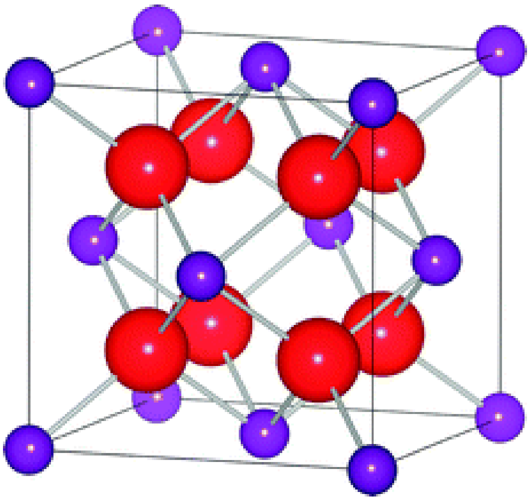

Figure 2.3 Crystal structure of CeO_2 [60].

Important applications of cerium oxide include:

- Catalysts and catalyst support
- Coatings for infrared filters
- Buffer layer for superconductors
- Coloring agents for plastic
- Infrared absorbents and sintering additives
- Oxidation resistant coatings, oxygen pumps and oxygen sensors
- Heat resistant alloy coatings
- Electrolyte and/or electrode materials for solid oxide fuel cells
- Polishing media for electronic devices, glasses, and bearing balls
- UV absorbent (absorption at ~ 400 nm is the strongest for any oxide)

Table 2.3 Physical and chemical properties of CeO_2.

Molecular Weight (g/mol.)	172.1142
Apparent Density (g/cm^3)	7.65 g/cm^3 as a solid
Specific Gravity	7.28
Melting Point (°C)	Approx. 2500 °C
Boiling Point (°C)	3500 °C
Odor	Odorless
Acute Health Hazard	Yes
Mohs Hardness @ 20 °C	6
EINECS Number	215-150-4
Solubility In Water	Insoluble
Appearance	White or pale yellow solid
Crystallography	Cubic, face centered

Several different research and development projects have focused on increasing the activity of metal catalysts. Most of the catalyst support used in water gas shift reaction is cerium oxide or CeO_2 because of its high oxygen storage capacity and cooperative effect of ceria-metal leading to highly active sites [29-31]. Many studies have shown that an addition of some metals onto ceria supports leads to an increase in catalytic activities of water gas shift reaction. The oxygen ion conductivity of gadolinia-doped ceria (GDC) solid solutions, typically with 10-20% substitution of Ce by Gd, is one of the highest in this class of ceria-based material [32, 33]. And Yttrium was selected because of ionic radius are similar close to Gadolinium [34] and yttrium can improve the thermal stability and anti-aging performance of CeO_2 [35]. Yttria-doped ceria (YDC) has relatively high electrical conductivity in all doped CeO2 material, although the association enthalpy between dopant cation and oxygen vacancy is a little large[36]. However, one of the main drawbacks of ceria-bases materials is that high temperatures are required to sinter the material to form a dense body. To fix this problem, different routes for the preparation of support powders have been proposed [37, 38]. There are many preparation method used to prepare ceria support; solid state [39], combustion [40], sol-gel [41], citrate complexation [42], co-precipitation [43], and etc. Which most of them used high temperature to calcine so hydrothermal synthesis [44] with used low temperature calcination is one of the method that interested to apply in this low temperature preparation method. And another popular technique used in doped ceria preparation technique is co-precipitation method because it was easy and not complicated. For metal doped ceria, found that gadolinium doped ceria used a lot in steam reforming for production of Hydrogen [45, 46] which it widely use in water gas shift reaction also.

In part of adding metal on to support, impregnation method was interest because of it easy and common used in this field. The selected of metal that doping on the support, focus on monometallic and bimetallic catalyst. After comparing between monometallic (Cu, Ni) and bimetallic (Cu-Ni), the monometallic gave higher percent hydrogen production [47]. To focus on monometallic, Ni is selected because it more active in water gas shift reaction [48]. After review through the literature reviews, there are few number study on the hydrogen production via water gas shift reaction with use gadolinium and yttrium doped ceria as a support catalyst.

In addition, other factors, such as temperature, percentage of metal use, etc. also have effects on the catalytic activity. Ta-Jen Huang et al. studied the hydrogen production over

$Cu/(Ce,Gd)O_{2-x}$ catalyst [49]. The temperature also effect the change of the variation as shown in Table 2.4. It showed that the conversion increase with an increase of temperature, the CO content is smallest at 240°C; this is in accordance with the largest CO_2 selectivity and the highest H_2 yield. Figure 2.4 shows that the conversion increase by the increasing of catalyst weight. The percentage of metal also effect the surface area and hence affecting the catalytic activity.

Table 2.4 Variations of conversion, formation rates of H_2, CO_2 and CO, H_2 yield, CO_2 selectivity and CO content with reaction temperature over 0.1 g of 5% GDC.

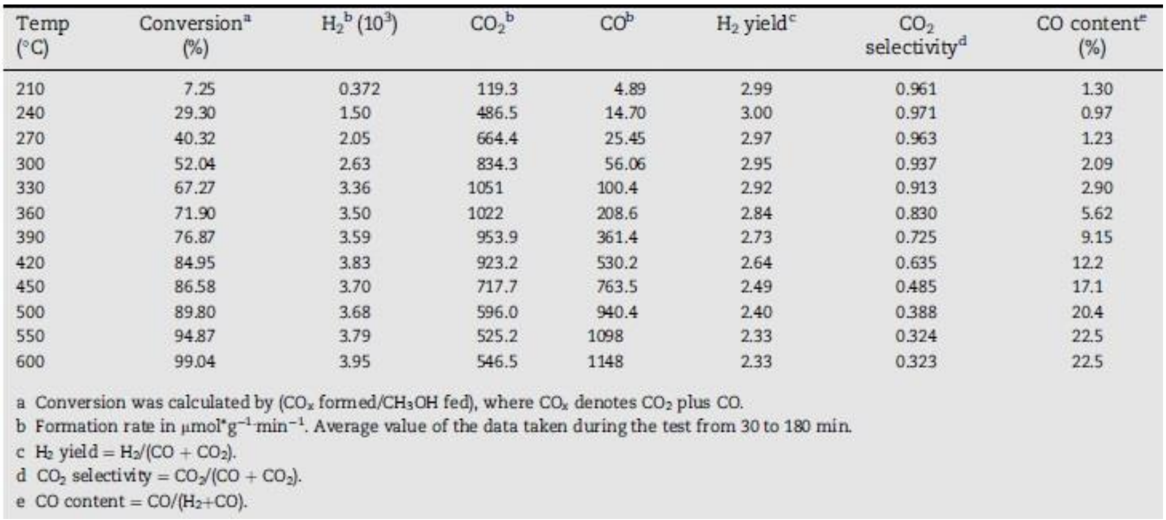

Temp (°C)	Conversion[a] (%)	H_2[b] (10^3)	CO_2[b]	CO[b]	H_2 yield[c]	CO_2 selectivity[d]	CO content[e] (%)
210	7.25	0.372	119.3	4.89	2.99	0.961	1.30
240	29.30	1.50	486.5	14.70	3.00	0.971	0.97
270	40.32	2.05	664.4	25.45	2.97	0.963	1.23
300	52.04	2.63	834.3	56.06	2.95	0.937	2.09
330	67.27	3.36	1051	100.4	2.92	0.913	2.90
360	71.90	3.50	1022	208.6	2.84	0.830	5.62
390	76.87	3.59	953.9	361.4	2.73	0.725	9.15
420	84.95	3.83	923.2	530.2	2.64	0.635	12.2
450	86.58	3.70	717.7	763.5	2.49	0.485	17.1
500	89.80	3.68	596.0	940.4	2.40	0.388	20.4
550	94.87	3.79	525.2	1098	2.33	0.324	22.5
600	99.04	3.95	546.5	1148	2.33	0.323	22.5

a Conversion was calculated by (CO_x formed/CH_3OH fed), where CO_x denotes CO_2 plus CO.
b Formation rate in $\mu mol^* g^{-1} min^{-1}$. Average value of the data taken during the test from 30 to 180 min.
c H_2 yield = $H_2/(CO + CO_2)$.
d CO_2 selectivity = $CO_2/(CO + CO_2)$.
e CO content = $CO/(H_2+CO)$.

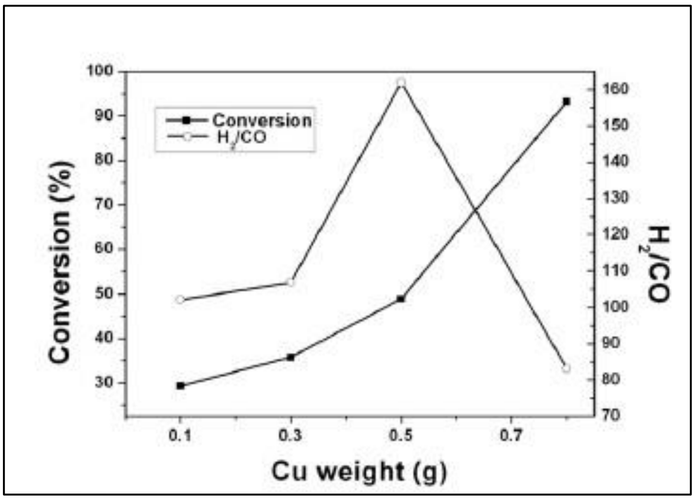

Figure 2.4 Effect of catalyst weight on conversion.

CHAPTER 3
METHODOLOGY

In this research, ceria-based samples were prepared by 2 different methods: low temperature method and co-precipitation method [50]. All materials were then examined for their specific surface area using Brunauer-Emmett-Teller (BET). X-ray diffraction (XRD) and Scanning Electron microscope (SEM) were used to determine the structure and morphology of samples. Temperature programmed reduction (TPR) was also used to find the most efficient reduction condition. All synthesized catalysts were tested toward water gas shift reaction under selected operating conditions.

3.1 Preparation of supports

3.1.1 Low temperature method

Nitrate salts of cerium and metal were dissolved in deionized (DI) water. Then, sodium hydroxide (NaOH) was added to make the solution pH equal to 10. The reactions were performed in a crucible at 260°C for 10 hours.

3.1.2 Co-precipitation method

For co-precipitation, nitrate salts of cerium, metal and urea (H_2NCONH_2) were mixed in DI water and solution was heated to 100°C under stirring. While heated, 2 ml of Sodium hydroxide (NaOH) was added dropwise until yellow precipitates were obtained. The suspension was stirred and heated at the same temperature for 4 hours, then filtered and washed twice with boiling deionized water. The filtered ceria precipitate was kept overnight at 110°C and then calcined at 450°C for 4 hours.

3.2 Preparation of catalyst

Monometallic based catalysts were prepared by the impregnation method. $Ni(NO_3)_2 \cdot 6H_2O$ was dissolved with the minimal amount of deionized water. The salts solution was added to Ce-M-O mixed oxide support. The catalyst were kept overnight at 110°C and then calcined in an oven at 650°C for 8 hours. Fig. 3.1 shows a summary or the support and catalyst preparation in our present study.

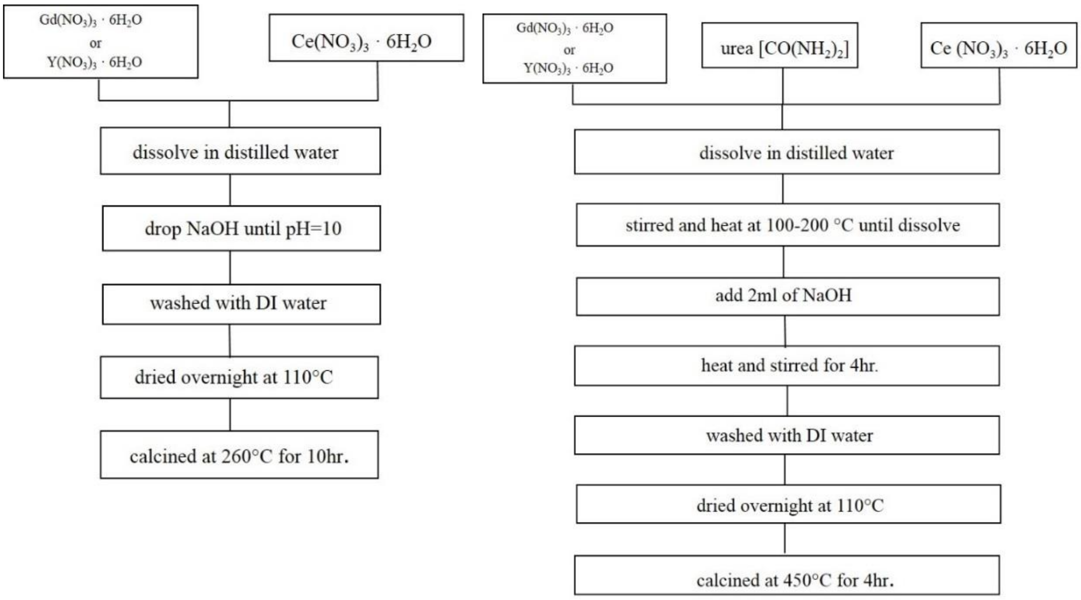

(a) (b)

Figure 3.1 Preparation process of supports and catalysts by (a) low temperature method and (b) Co-precipitation method.

3.3 Catalyst testing

3.3.1 Reactivity toward water gas shift reaction

Catalyst activity test was carried out over wide range temperatures, increased from 100°C to 500°C. The reaction was performed in the flow reactor. Gas mixture of 5% CO, 10% H_2O in balanced N_2 of the total flow rate 100 ml/min was controlled using mass flow controllers. The input gases were passed into the tube reactor, which was loaded with catalysts. The reactor was situated inside a tube furnace which controlled the temperature of reactor. Reaction occurs in the reactor and the outlet gas was analyzed by on-line gas chromatography equipped with a TCD analyzer (Fig. 3.2).

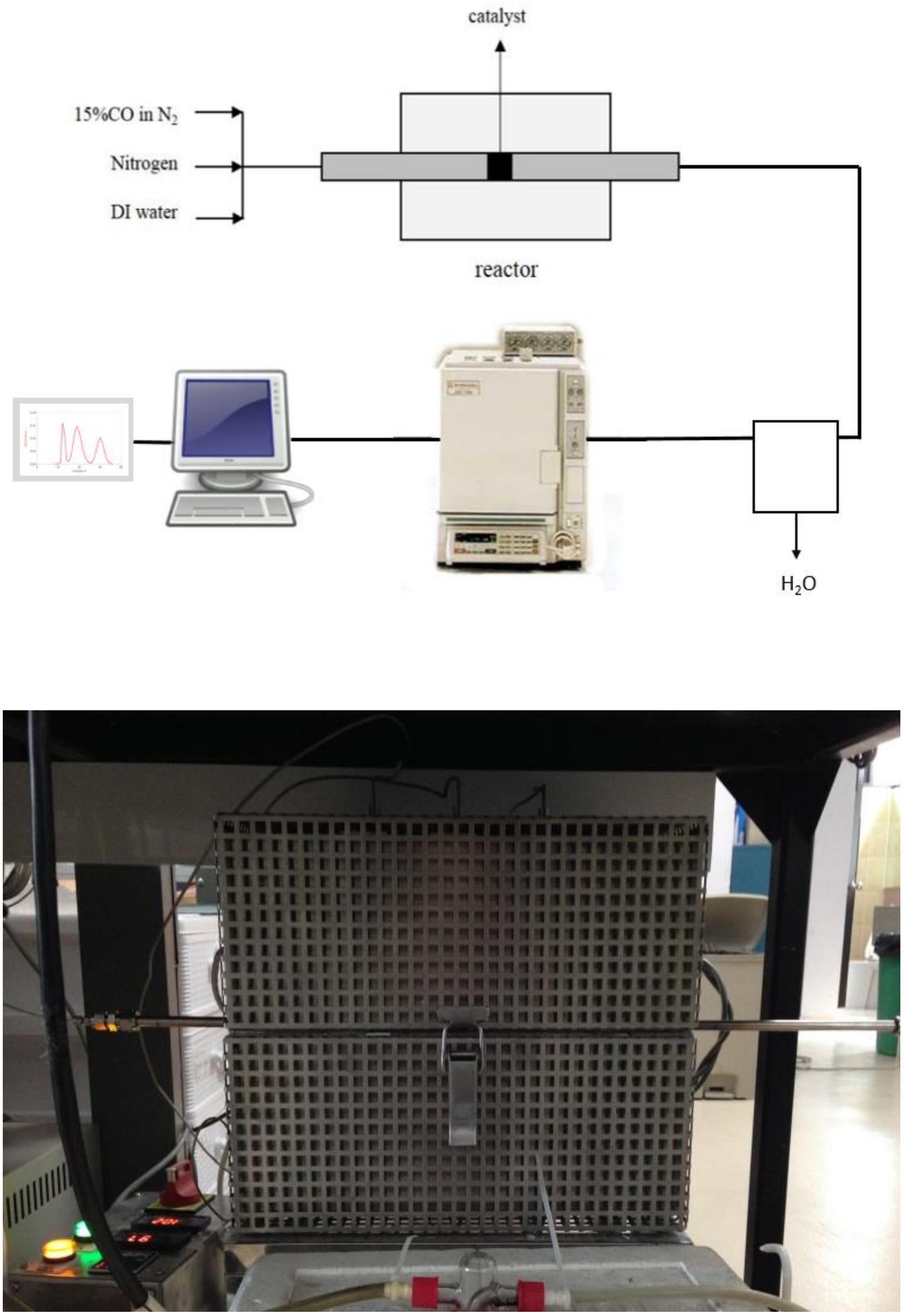

Figure 3.2 Process of water gas shift reaction

The catalytic activity was calculated by the equation:

$$\%CO\ conversion = \frac{CO_{in}-CO_{out}}{CO_{in}} \times 100 \tag{16}$$

3.3.2 Kinetics of water gas shift reaction

The kinetics of water gas shift over all ceria were studied by performing the experiments at different temperatures and fitting the correlation of the reaction rate with reaction temperatures by Arrhenius Equation ($k = Ae^{-Ea/RT}$). And the kinetics of reaction order were investigated by varying percentage of inlet carbon dioxide (CO_2) and Hydrogen (H_2) at 400 °C. While the percentage of carbon monoxide (CO) and nitrogen (N_2) were kept constant at 1%CO for the effect of H_2 and 5%CO for the effect of CO_2.

3.4 Catalyst Characterization

3.4.1 X-Ray Diffraction (XRD)

X-ray Diffraction techniques are a family of non-destructive analytical techniques that reveal information of the crystallographic structure, chemical composition, and physical properties of materials and thin films. Powder diffraction XRD is a technique used to characterize the crystallographic structure, crystallite size (grain size), and preferred orientation in polycrystalline or powder solid samples. Powder diffraction is commonly used to identify unknown phases of substances, by comparing diffraction data against a database maintained by the international Centre for Diffraction Data. It may also be used to characterize heterogeneous solid mixtures to determine relative abundance of crystalline compounds, and when coupled with lattice refinement technique, such as Rietveld refinement, it can provide structural information of unknown materials.

The XRD technique is used to determine the crystal structure and composition of the specimens with nickel-filtered Cu Kα radiation (λ=1.54056 Å). X-ray generator under ambient conditions. The accelerating voltage was set at 40 kV, with 40 mA fluxes at a scanning rate of 0.02° per step and 0.5 s per step in the range of 20-80°. The crystallite size of ceria is calculated using Scherrer's equation.

$$D_{hkl} = \frac{0.9\lambda}{\beta\cos\theta} \tag{17}$$

Where D_{hkl} is the crystallite size, λ is the wavelength of radiation used, β is the line broadening of the peak or full0width at half maximum and θ is the angle of the diffraction peak.

Figure 3.3 X-Ray Diffraction (XRD)

3.4.2 Scanning electron microscope (SEM)

A SEM is one of the most versatile instruments available for the examination and analysis of the microstructural characteristics of solid objects. It provides 2 outstanding improvements over the optical microscope: it extends the resolution limits and improves the depth-of-focus resolution more dramatically. It was also capable of examining objects at a large range of magnifications. The coupling of an energy-dispersive x-ray detector to an SEM makes it possible to obtain topographic, crystallographic, and compositional information rapidly, efficiently, and simultaneously for the same area.

Figure 3.4 Scanning elctron microscope (SEM)

A finely focused electron beam scanned across the surface of the sample generates secondary electrons, backscattered electrons, and characteristic x-rays. These signals are collected by detectors to form images of the sample displayed on a cathode ray tube screen. Features seen from the SEM image may then be immediately analyzed for elemental composition using EDS or WDS. Secondary Electron Imaging shows the topography of surface features a few nm across. Films as thin as 20 nm produce adequate contrast images. Materials are viewed at useful magnifications up to 100,000x without the need for extensive sample preparation and without damaging the sample. Even higher magnifications and resolution are routinely obtained by our Field Emission SEM. Backscattered Electron Imaging shows the spatial distribution of elements or compounds within the top micron of the sample. Features as small as 10 nm are resolved and composition variations of as little as 0.2% determined. Data Output is generated in real time on the CRT monitor. Images and spectra can be obtained.

3.4.3 Brunauer Emmett Teller (BET)

The BET method was applied to determine the specific surface area of a powder by the physical adsorption of gas on the surface of the solid and by calculating the amount of adsorbate gas corresponding to a monomolecular layer on the surface. Physical adsorption results from relatively weak forces (van der Waals forces) between the adsorbate gas molecules and the adsorbent surface area of the test powder. The determination is usually carried out at the temperature of liquid nitrogen. The amount of gas adsorbed can be measured by a volumetric or continuous flow procedure.

The BET equation is applicable at low P/P_0 range and it is written in linear form:

$$\frac{1}{V[(P_0/P)-1]} = \frac{C-1}{V_m c}\left(\frac{P}{P_0}\right) + \frac{1}{V_m c} \qquad (18)$$

where P = partial vapour pressure of adsorbate gas in equilibrium

P_o = saturated pressure of adsorbate gas

V = volume of gas adsorbed at standard temperature and pressure (STP) [273.15 K and atmospheric pressure (1.013 × 105 Pa)]

V_m = volume of gas adsorbed at STP to produce an apparent monolayer on the sample surface, in millilitres

C = dimensionless constant that is related to the enthalpy of adsorption of the adsorbate gas on the powder sample.

Figure 3.5 Brunauer Emmett Teller (BET)

3.4.4 Temperature programmed reduction (TPR)

TPR is a technique for the characterization of solid materials to find the most efficient reduction conditions. An oxidized catalyst precursor is submitted to a programmed temperature rise while a reducing gas mixture is flowed over it [55]. A simple container (U-tube) is filled with a catalyst. This sample vessel is positioned in a furnace with temperature controlled equipment. A thermocouple is placed in the solid for the temperature measurement. To remove the present air, the container is filled with an inert gas (Argon). The composition of the gaseous mixture is measured at the exit of the sample container with appropriate detectors (thermal conductivity detector). A reduction takes place at a certain temperature when hydrogen is consumed, which is recorded by the detector. H_2 temperature programmed reduction or H_2-TPR was carried out on a Quantachrome Autosorp-1-C instrument. TPR experiments were performed under a flow of 3.5%H_2/Ar mixture over 0.05 g of catalyst from room temperature to 650°C using a heating rate of 10 °C/min. Prior to TPR, the catalysts were treated under high purity Argon gas at 120°C for 30 min.

Figure 3.6 BELCAT-B model

CHAPTER 4
RESULTS AND DISCUSSION

4.1 Phase structure, particle size and morphology of the powders

The XRD patterns of all catalysts are shown in Figures 4.1 – 4.4. The fluorite oxide-type diffraction of CeO_2 was observed in all samples. CeO_2 appeared to be phase-pure with cubic crystallography. Peak identifications were made with reference to the JCPDS file Nos. 34-0394, 75-0161, 75-0162, 75-0174 and 75-0175 respectively. All main reflections of a typical cubic fluorite structure, corresponding to (111), (200), (220), (311), (222), (400), (331) and (420) planes in the 2θ scanning range 20-80° were found in every prepared powder. These patterns indicate that the GDC and YDC formed solid solutions in the fluorite structure of ceria with Gd and Y substitutions. The absence of other reflection in Gd-doped ceria and Y-doped ceria indicates that Gd and Y incorporates into subsurface region of CeO_2 lattice to form solid solution. The diffraction peaks of Gd-doped ceria (28.464°) and Y-doped ceria (28.459°) appear at slightly lower diffraction angle compared with the diffraction peaks of CeO_2 (28.479°). An addition of Ni did not cause any other observable peak in the XRD reflection of ceria, Gd-doped ceria and Y-doped ceria. The result suggests that nickel oxide is highly dispersed on the surface or support [51]. The average crystallite sizes of ceria and modified ceria, calculated from x-ray line broadening using Scherer's equation, are compiled in Table 4.1. Doping CeO_2 with gadolinium and yttrium led to a reduction of crystallite size in case of low temperature method but it increased the crystallite size for co-precipitation method. As expected, the surface area decreased at high temperatures. However, the value of 20YDC in low temperature method was still suspicious.

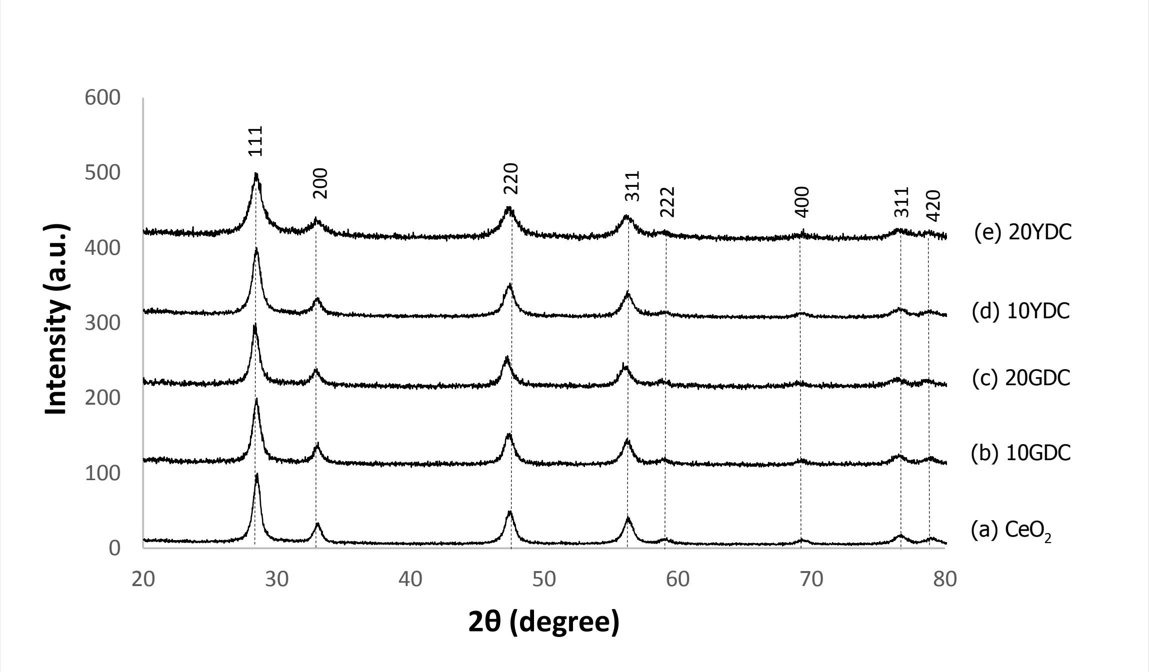

Figure 4.1 XRD patterns of support synthesized by low temperature method.

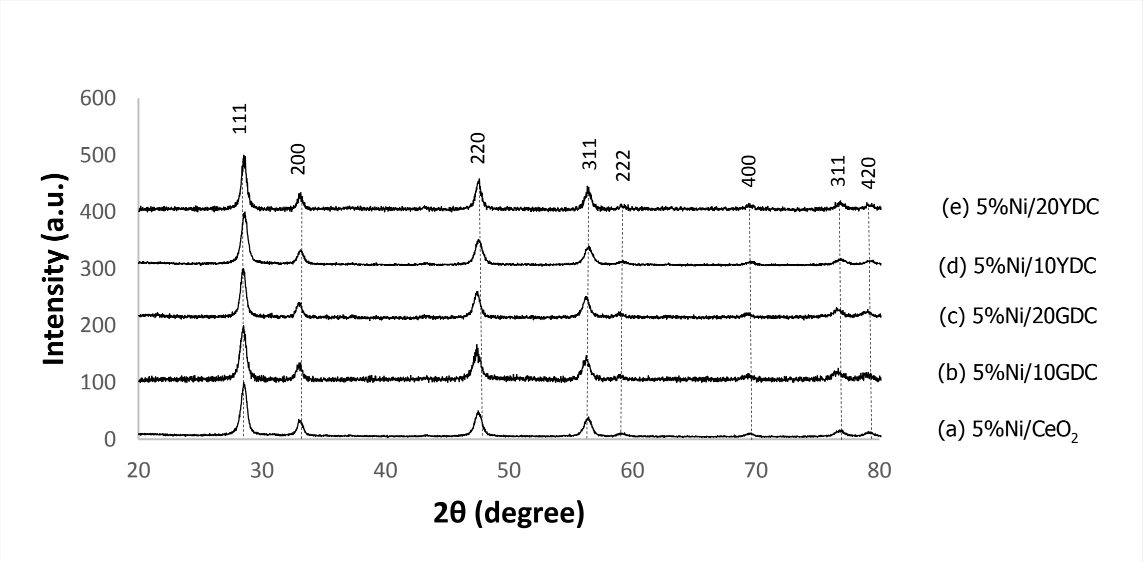

Figure 4.2 XRD patterns of catalysts synthesized by low temperature method.

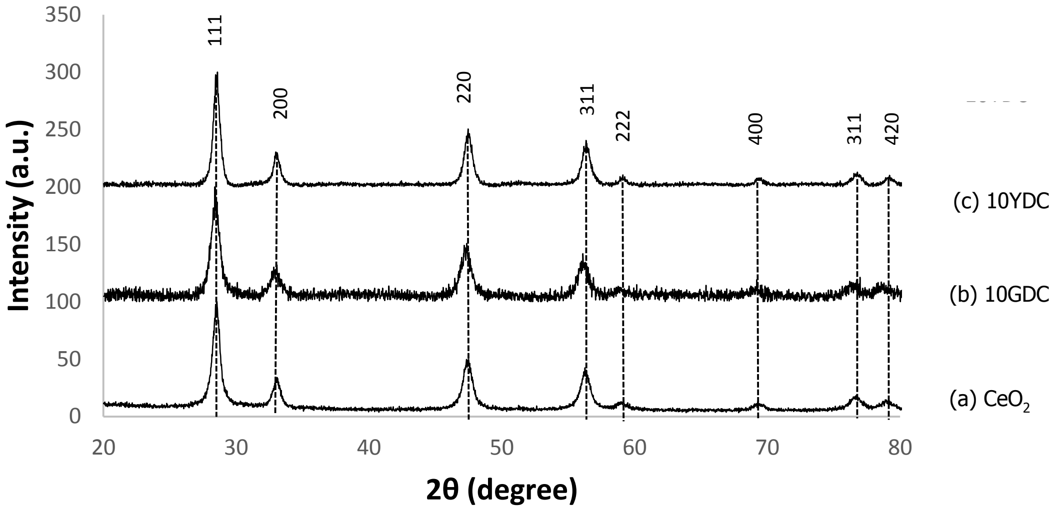

Figure 4.3 XRD patterns of support synthesized by co-precipitation method.

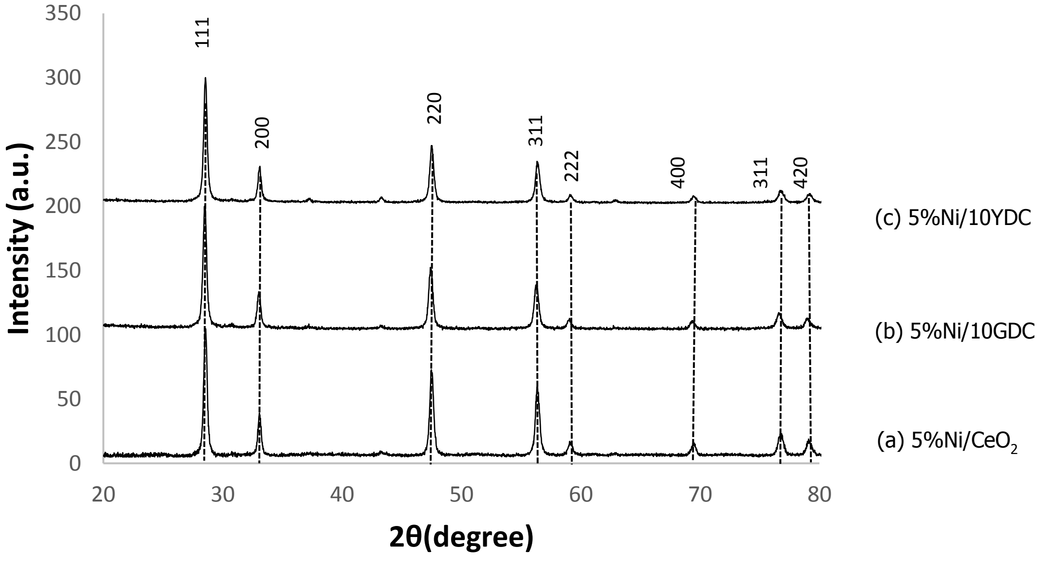

Figure 4.4 XRD patterns of catalyst synthesized by co-precipitation method.

Table 4.1 Crystallite sizes of catalysts prepared by (a) low temperature method and (b) co-precipitation method.

Powder	**Crystallite size (D)**
CeO_2	12.7726
10GDC	11.6288
20GDC	12.0173
10YDC	11.0883
20YDC	8.1732
5%Ni-CeO_2	14.4512
5%Ni-10GDC	14.1635
5%Ni-20GDC	16.4414
5%Ni-10YDC	14.0270
5%Ni-20YDC	16.2579

(a)

Powder	**Crystallite size (D)**
CeO_2	12.8877
10GDC	13.1441
10YDC	13.6242
5%Ni-CeO_2	25.7906
5%Ni-10GDC	24.2611
5%Ni-10YDC	25.7905

(b)

Table 4.2 Surface area of catalysts prepared by (a) low temperature method and (b) co-precipitation method.

Powder	**Surface area (m^2/g)**
CeO_2	77.01
10GDC	76.06
20GDC	37.23
10YDC	66.13
20YDC	109.5
5%Ni-CeO_2	33.32
5%Ni-10GDC	49.14
5%Ni-20GDC	22.85
5%Ni-10YDC	44.86
5%Ni-20YDC	10.73

(a)

Powder	**Surface area (m^2/g)**
CeO_2	63.83
10GDC	79.84
10YDC	26.94
5%Ni-CeO_2	12.27
5%Ni-10GDC	14.32
5%Ni-10YDC	8.291

(b)

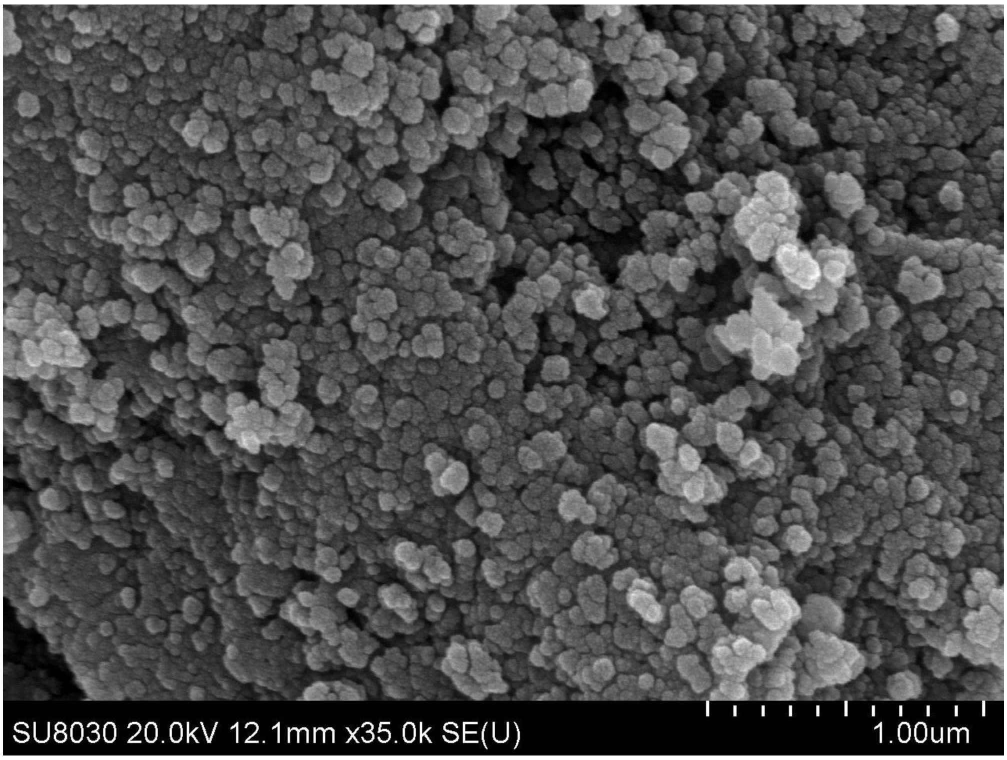

Figure 4.5 SEM micrograph of CeO_2 prepared by low temperature method and calcined at 260°C.

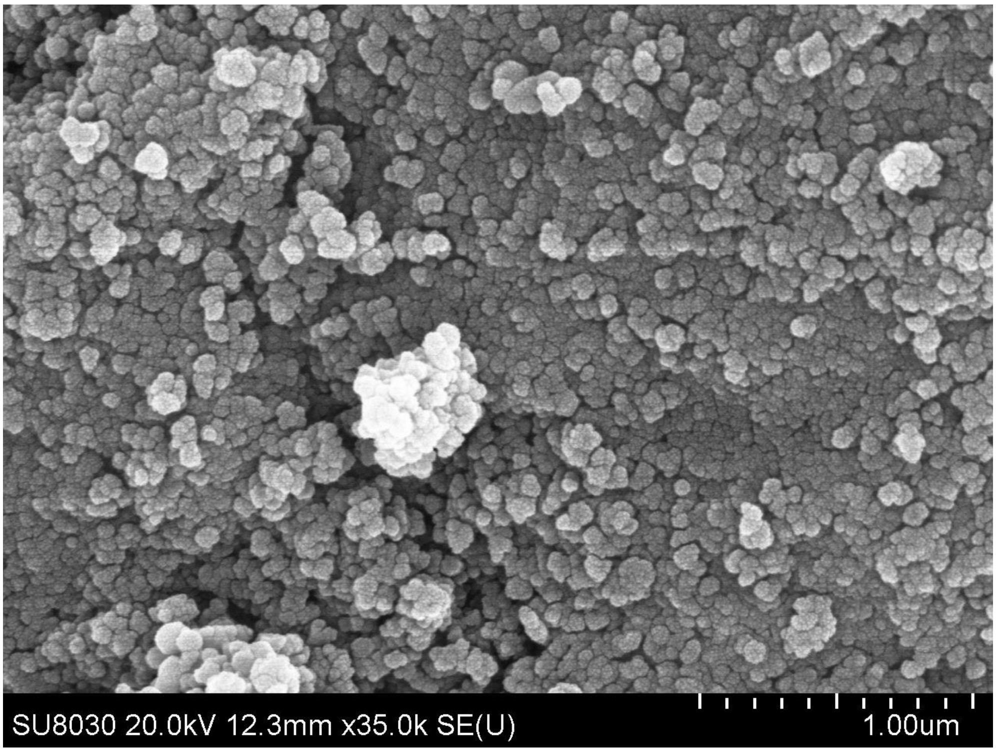

Figure 4.6 SEM micrograph of 5%Ni/CeO_2 prepared by low temperature method and calcined at 650 °C.

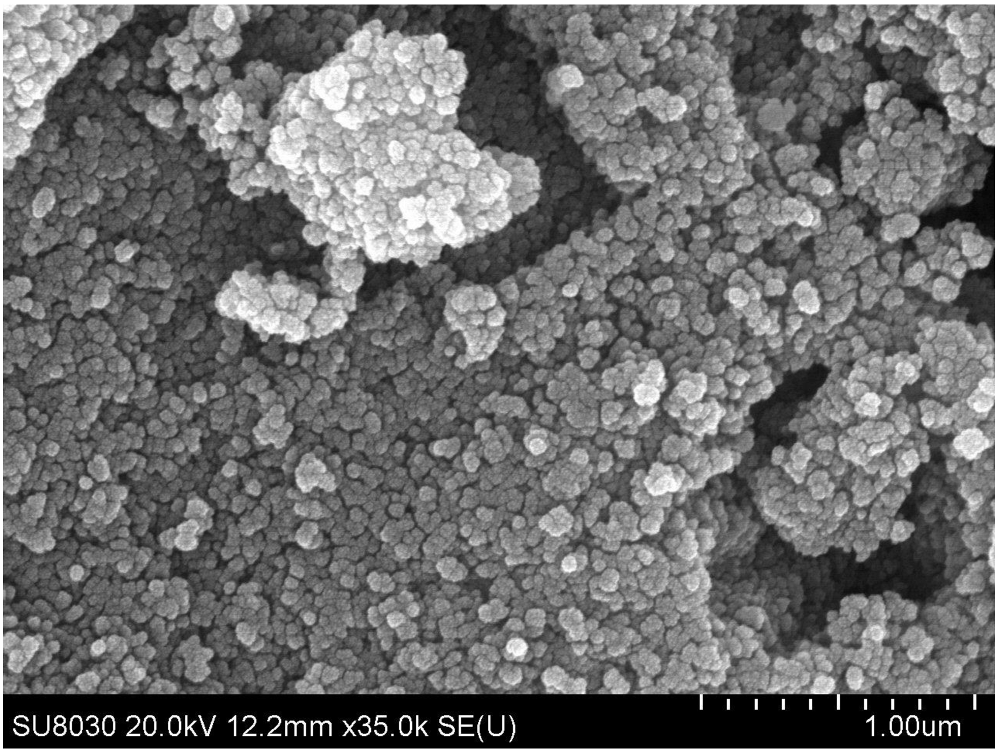

Figure 4.7 SEM micrograph of CeO_2 prepared by co-precipitation method and calcined at 450°C.

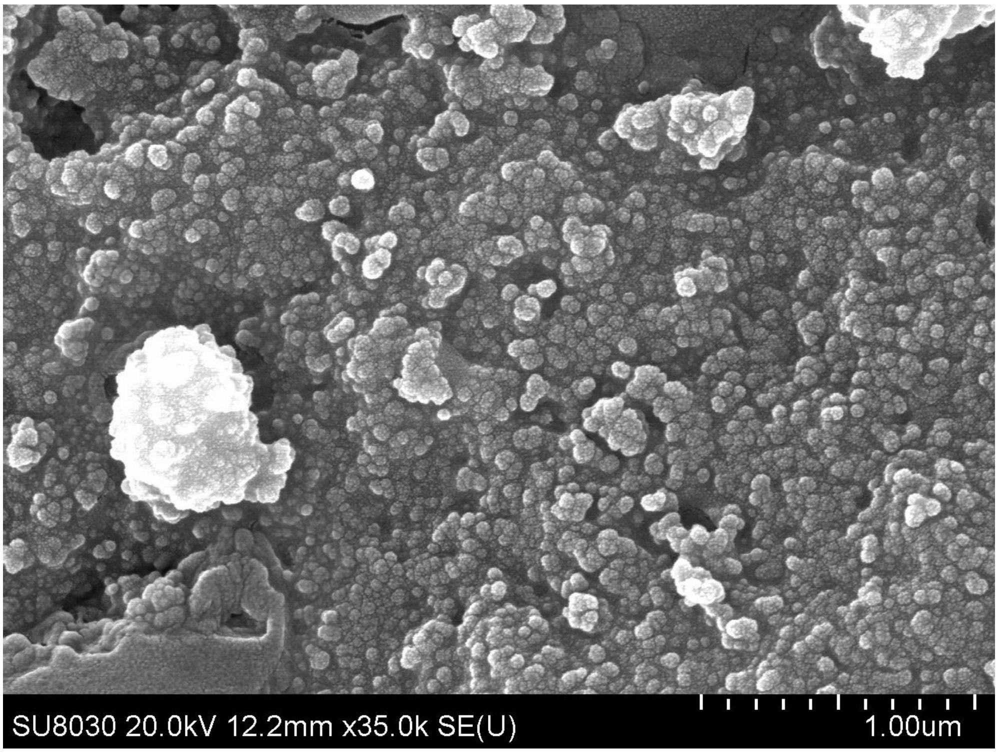

Figure 4.8 SEM micrograph of 5%Ni/CeO_2 prepared by co-precipitation method and calcined at 650°C.

Significantly, in spite of the different preparation processes, ceria and doped ceria of both methods gave nearly the same morphology (Figures 4.5 – 4.8). From the observation of both preparation methods, a doped ceria catalyst was packed tightly. To investigate the dispersion of Ni, Energy Dispersive X-ray Spectroscopy (EDS) in the mode of elemental mapping and line scan function were used. The results of elemental mapping are shown in Figures 4.9 - 4.10.

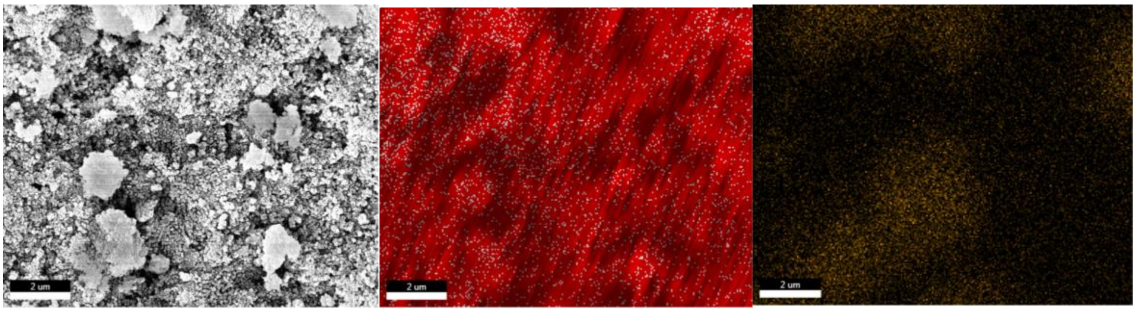

Figure 4.9 EDS figure of 5%Ni/CeO_2 prepared by low temperature method.

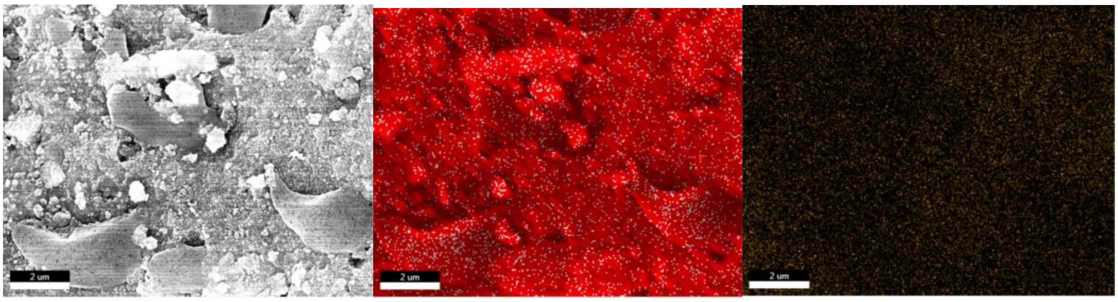

Figure 4.10 EDS figure of 5%Ni/CeO_2 prepared by co-precipitation method.

According to the EDS in the function of elemental mapping results, the dispersion of Ni prepared by co-precipitation method is better than that of Ni prepared by low temperature method. Another function of SEM to confirm the Ni dispersion is shown in Figures 4.11 and 4.12. EDS line scan function that crosses through the round particle in SEM shows elemental profile plot, from which Ni and Ce particles can be clearly detected.

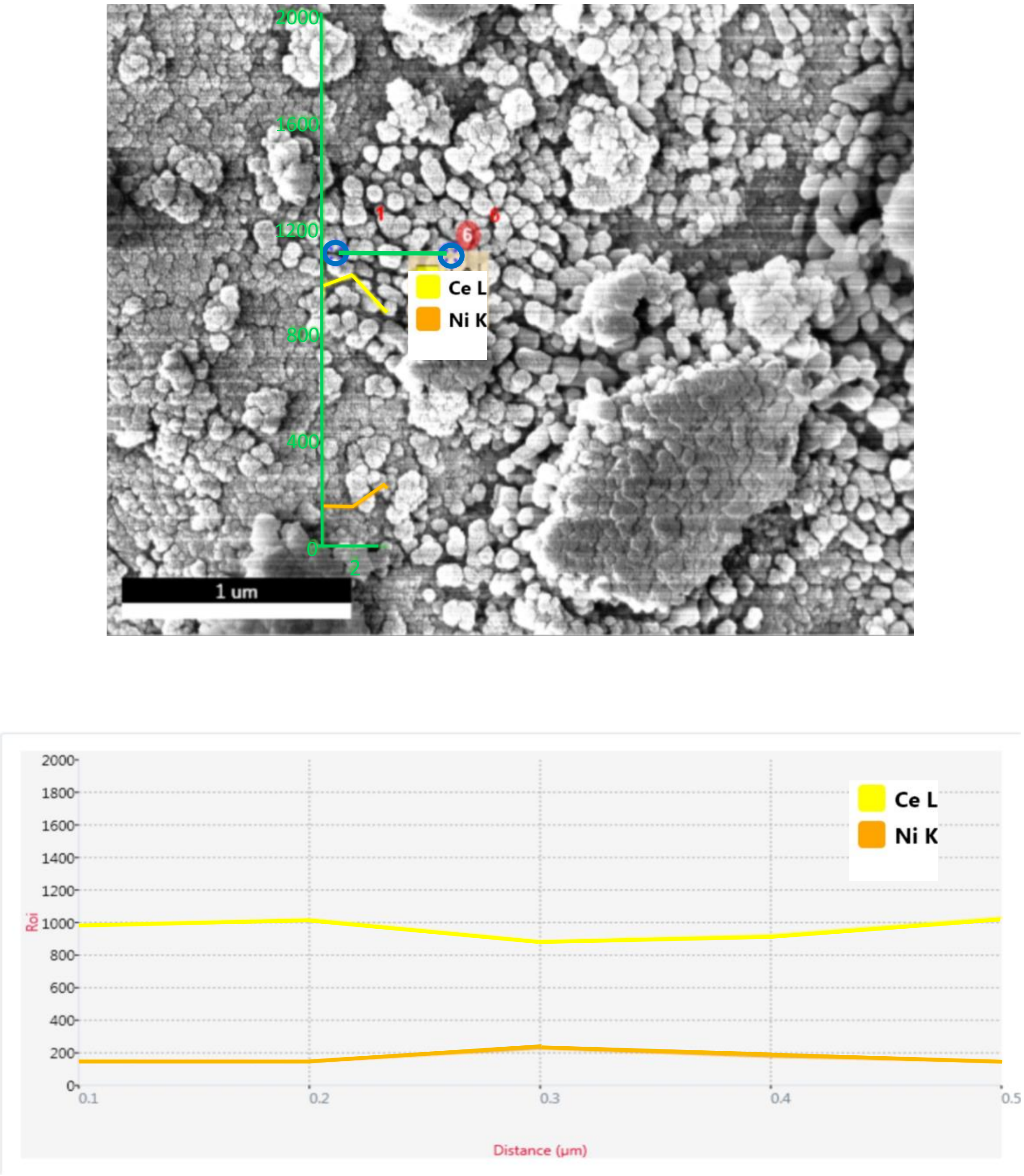

Figure 4.11 EDS line of 5%Ni/CeO_2 prepared by low temperature method.

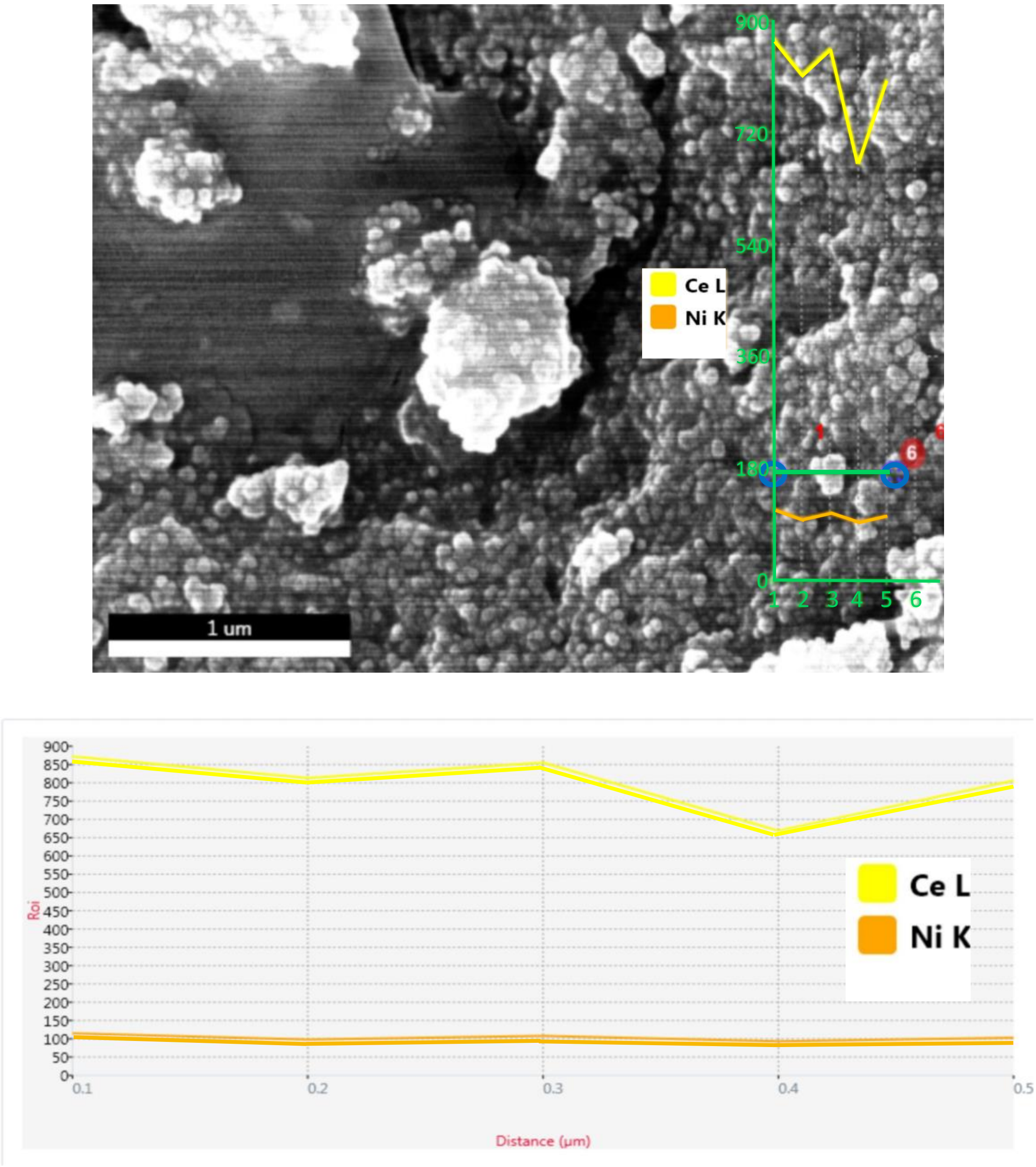

Figure 4.12 EDS line of 5%Ni/CeO_2 prepared by co-precipitation method.

4.2 Catalytic Reactivity

Figures 4.13 and 4.14 compare activity of supports: CeO_2, 10GDC, 20GDC, 10YDC and 20YDC and catalysts; 5%Ni/CeO_2, 5%Ni/10GDC, 5%Ni/20GDC, 5%Ni/10YDC and 5%Ni/20YDC synthesized by low temperature method. It appears that after Ni doping, the activity of all materials significantly increase. Similar trend was also observed from the catalysts prepared by co-precipitation method (as presented in Figures 4.15 and 4.16). It can be seen that the catalyst activity (in term of CO conversion) increases with increasing the reaction temperature from 100°C to 350-400°C. At higher reaction temperature (450-500°C), the CO conversion decreased with increasing the reaction temperature, which could be due to reaching of reaction equilibrium. Therefore, the suitable temperature for the water gas shift reaction over these catalysts appears to be in the range of 350-400°C. Among all catalysts, Ni over CeO_2 prepared by a precipitation technique yielded the highest CO conversion of 92% at 400°C.

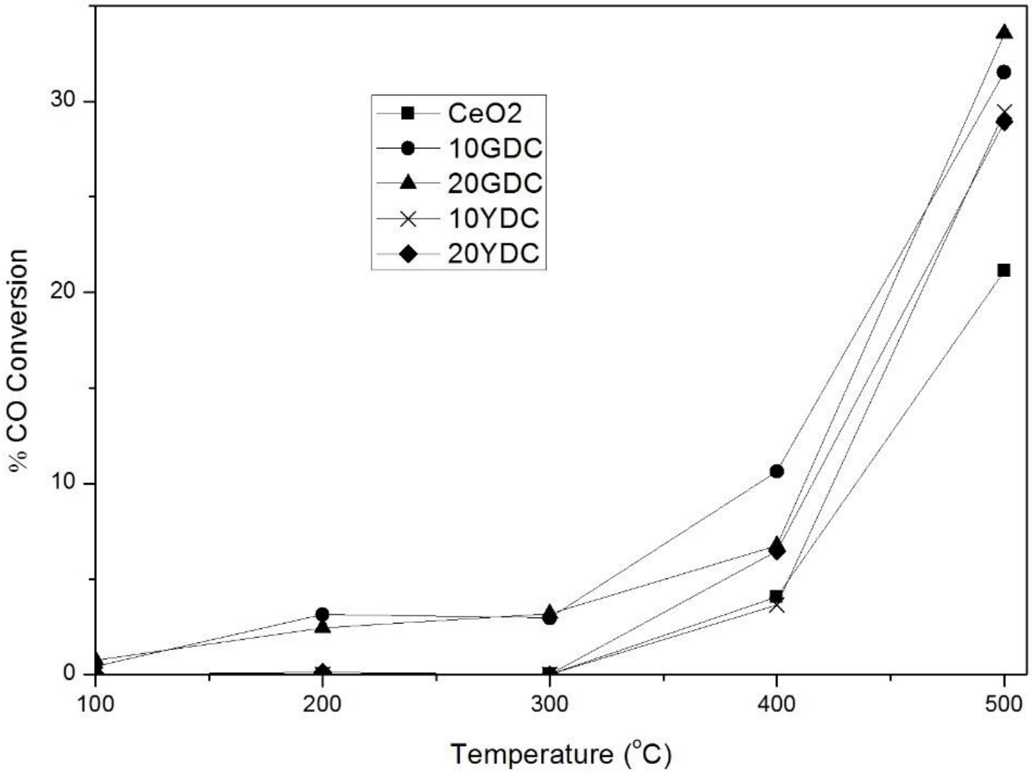

Figure 4.13 Water gas shift activity of various supports prepared by low temperature method.

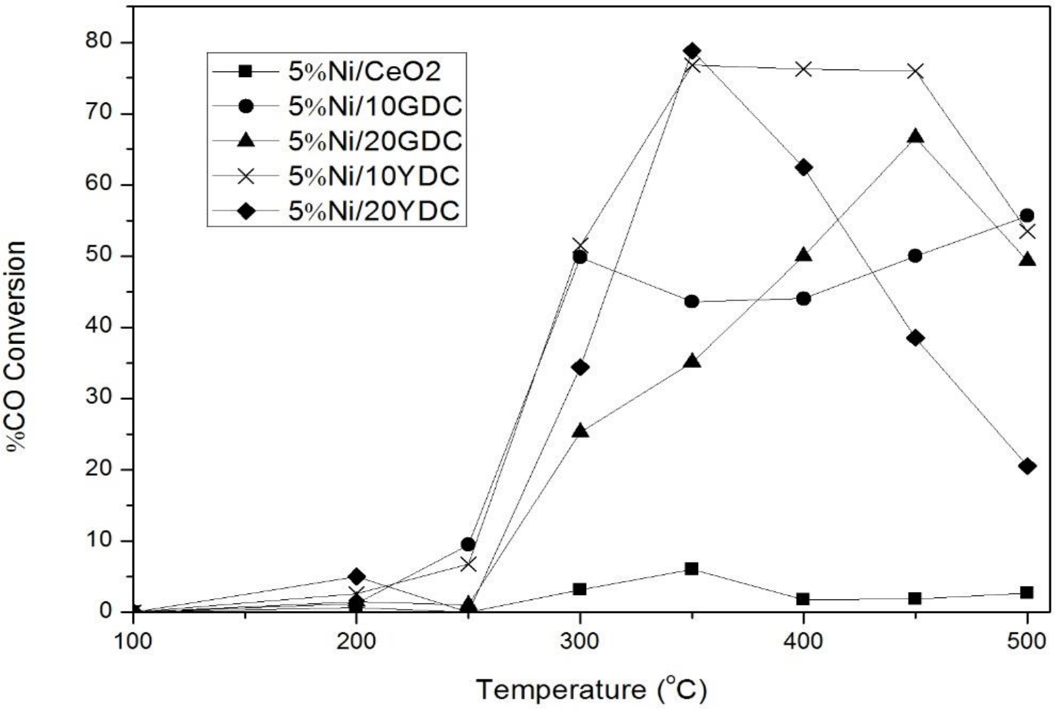

Figure 4.14 Water gas shift activity of various catalysts prepared by low temperature method.

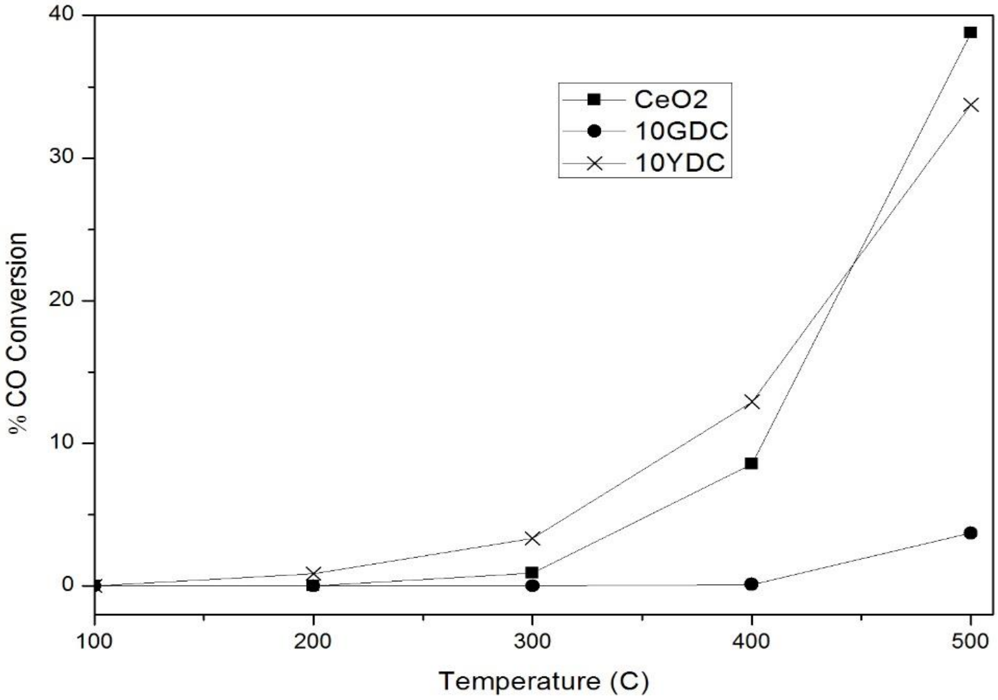

Figure 4.15 Water gas shift activity of various supports prepared by co-precipitation method.

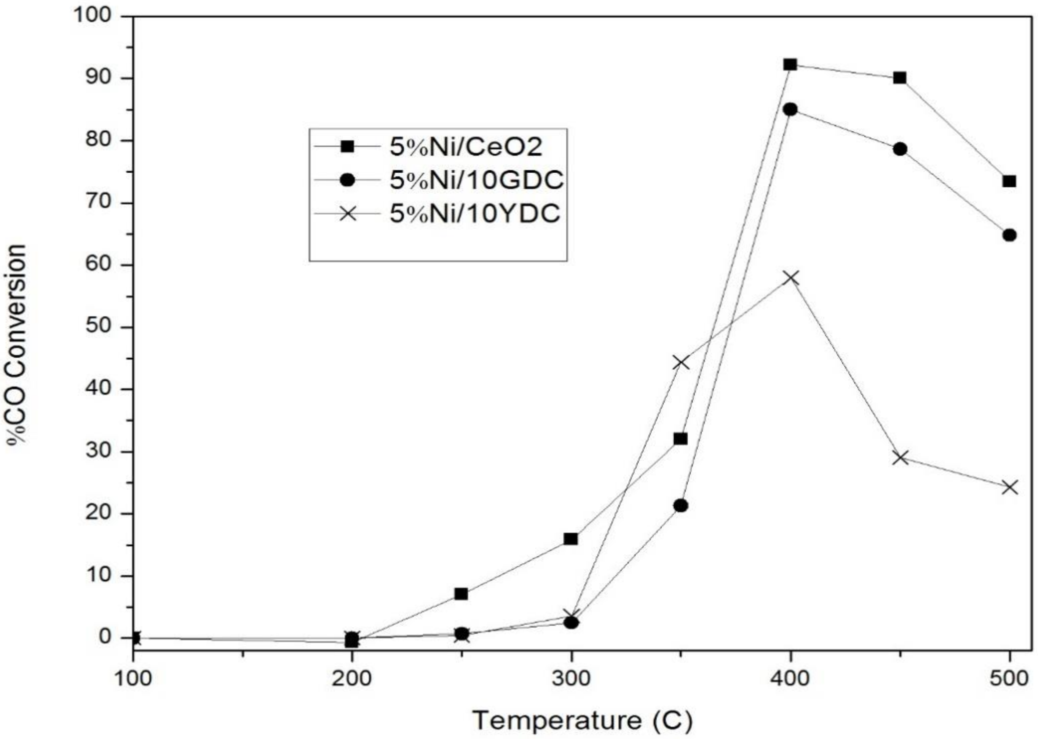

Figure 4.16 Water gas shift activity of various catalysts prepared by co-precipitation method.

4.3 Temperature programmed reduction

H_2-TPR profiles of ceria, GDC, YDC and doped ceria are presented in Figures 4.17 - 4.20. An addition of Ni onto ceria and doped ceria drastically affects the surface reduction toward lower temperature. For the group of catalysts synthesized by a low temperature method and co-precipitation, it is clearly shown that after doping with Ni, the reduction temperature decreases. Therefore, this investigation confirms that the reaction can take place easier when Ni is impregnated over CeO_2-based materials. For instance, for 10YDC prepared by low temperature technique, the reduction temperature was at 450°C. After doping with 5%Ni, the reducing temperature decreased to 350°C. Similar trend of the water gas shift activity was observed, from which the CO conversion increased from less than 5% for 10YDC to 75% for 5%Ni/10YDC at 400°C. In case of co-precipitation, 10YDC gave the reduction temperature at 460°C but for 5%Ni/10YDC, the reduction temperature appeared at 350°C. Similar trend of the water gas shift activity was also observed, from which the CO conversion increased from 13% for 10YDC to 60% for 5%Ni/10YDC at 400°C.

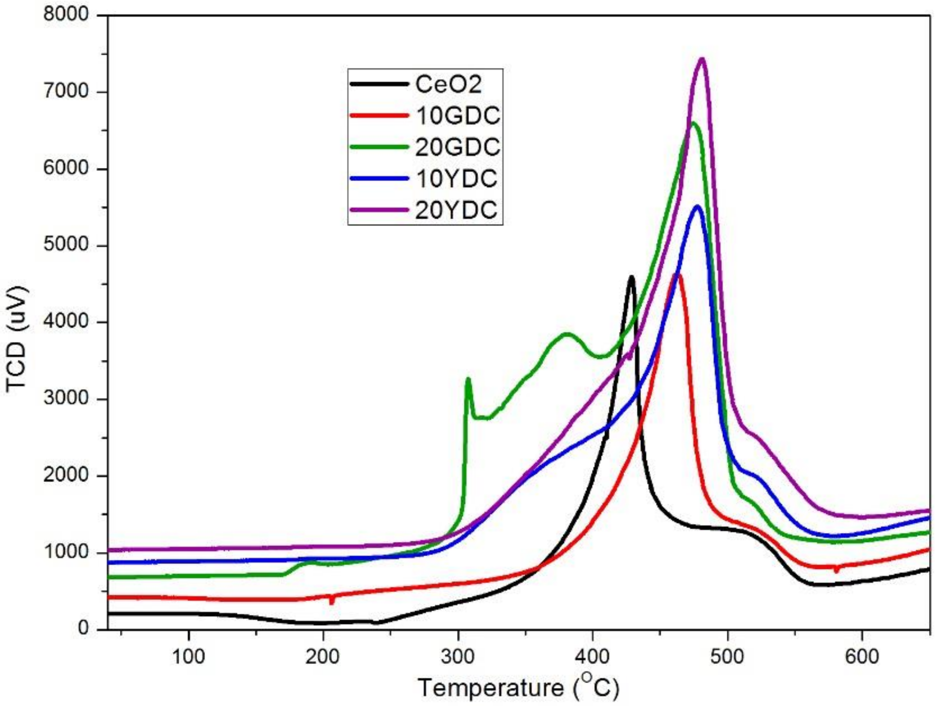

Figure 4.17 TPR of various supports synthesized by low temperature method.

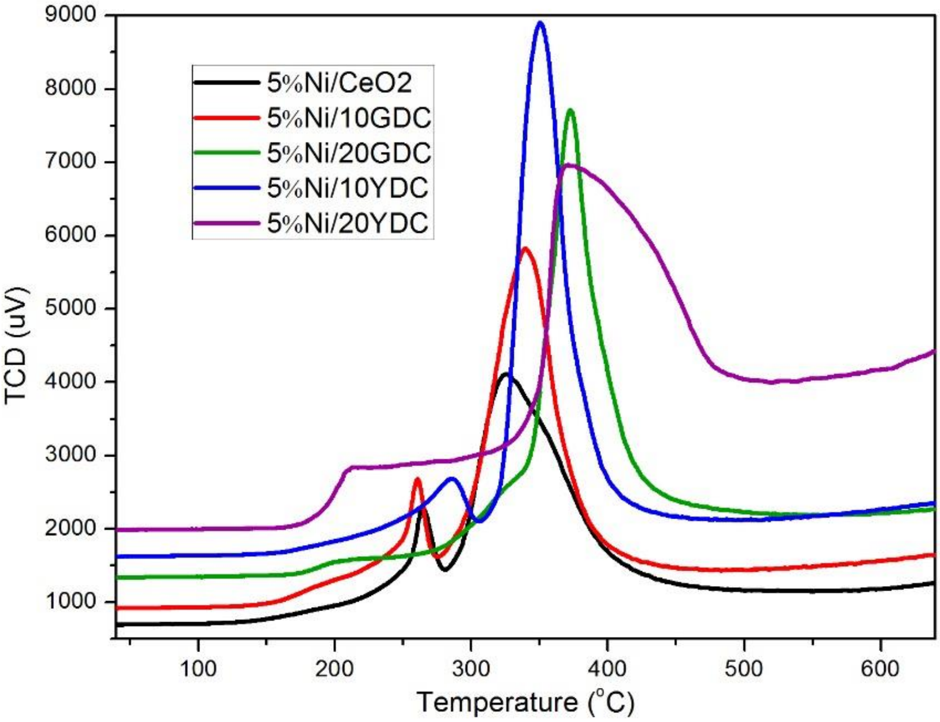

Figure 4.18 TPR of various catalysts synthesized by low temperature method.

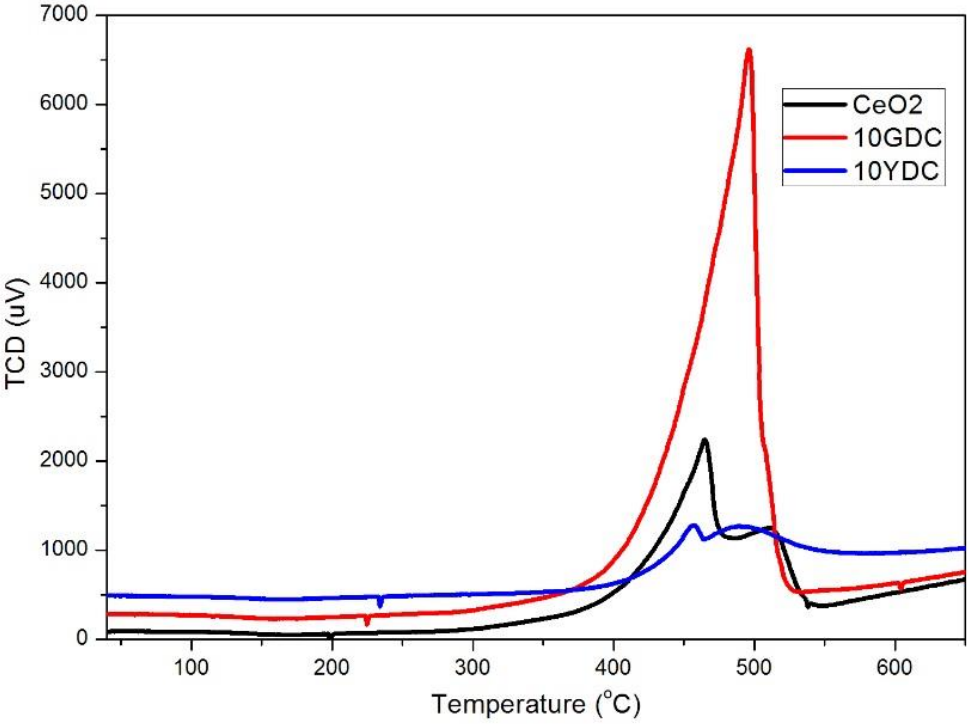

Figure 4.19 TPR of various supports synthesized by co-precipitation method.

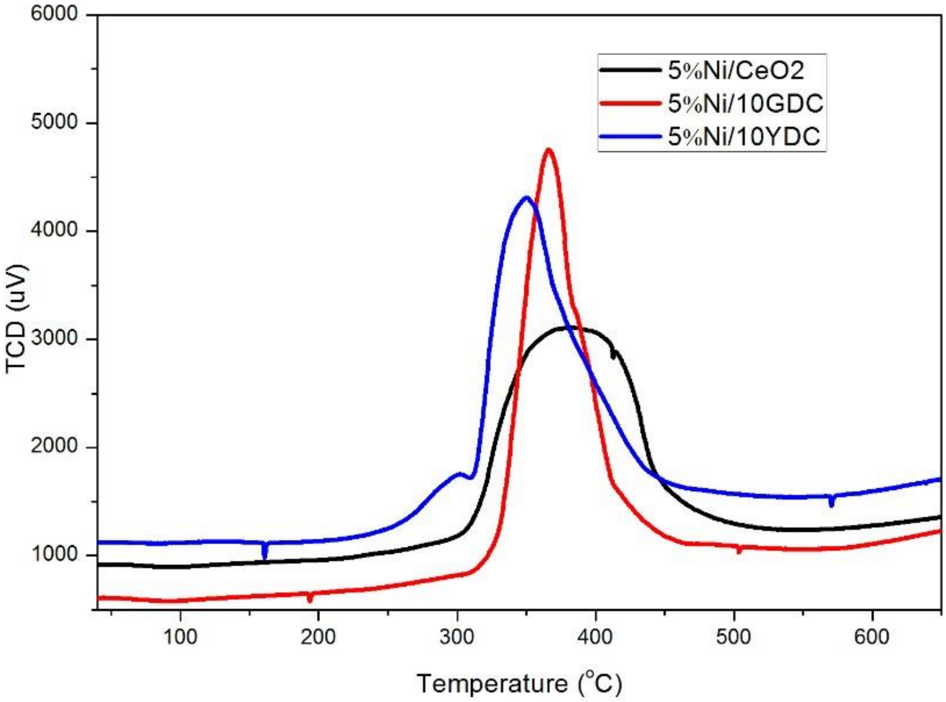

Figure 4.20 TPR of various catalysts synthesized by co-precipitation method.

4.4 Kinetics of water gas shift reaction

The activation energy and reaction orders of H_2, CO and CO_2 were predicted by the kinetic study. The activation energy can be obtained by performing the experiments at different temperatures and fitting the correlation of reaction rate with reaction temperature by Arrhenius equation ($k = Ae^{-Ea/RT}$). According to the Arrhenius plot of 5%Ni/CeO_2 as seen in Figure 4.21, the activation energy (E_a) is 27 kJ/mol.

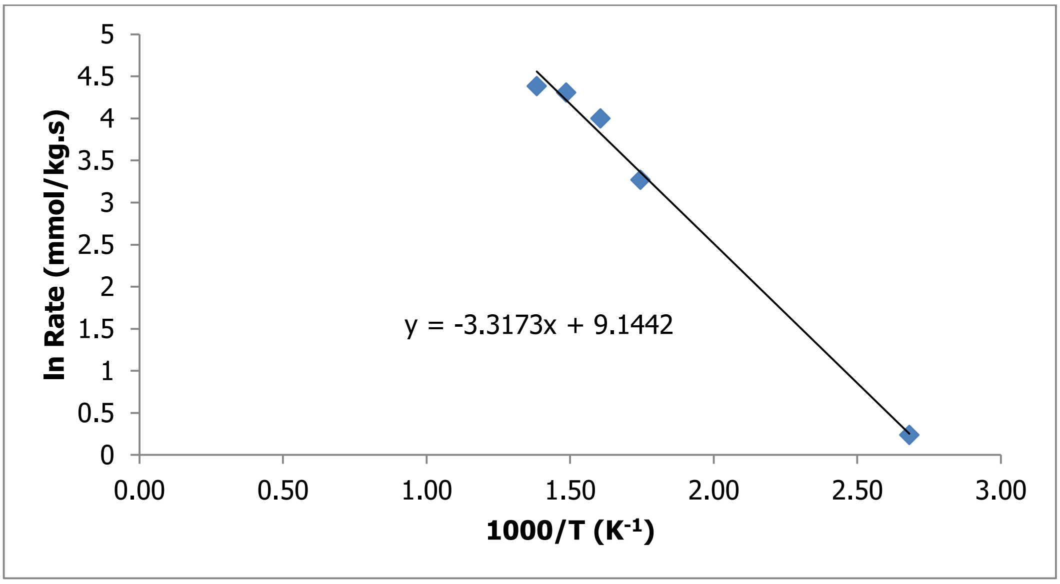

Figure 4.21 Arrhenius plot of 5%Ni/CeO_2.

To identify the reaction orders of H_2, CO and CO_2, the experiments were conducted at different inlets of H_2, CO and CO_2 concentrations under the same reaction temperature. As shown in Figures 4.22 - 4.24, it was found that the reaction order of CO was 0.69, whereas the reaction orders of H_2 and CO_2 were -0.13. This indicates the weak negative effects of H_2 and CO_2 on the reaction due to the promotion of reverse water gas shift reaction by both compounds.

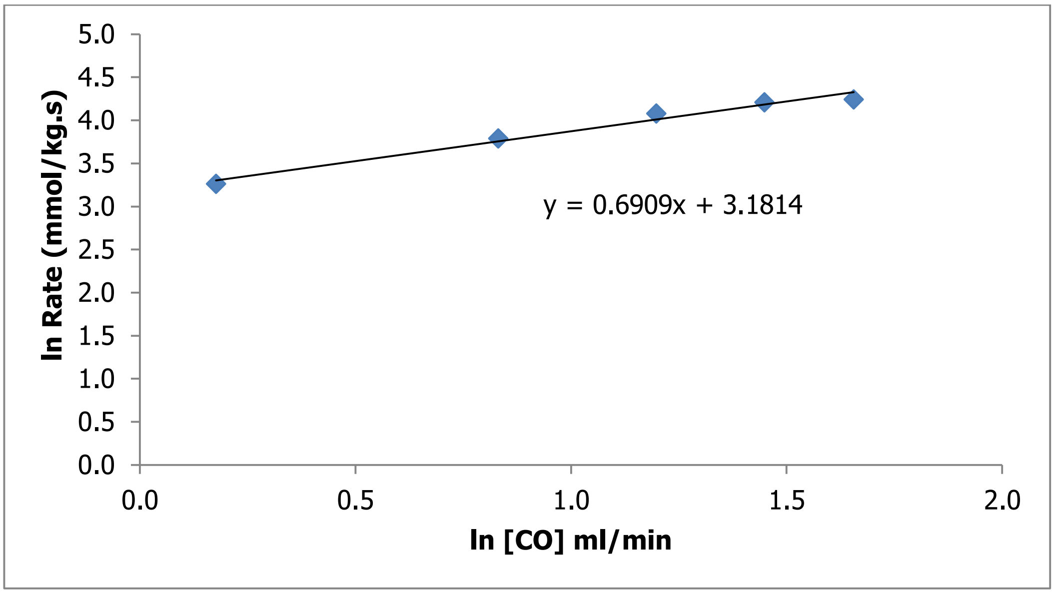

Figure 4.22 Reaction order of CO for 5%Ni/CeO_2 (using the inlet conditions of 1-5% CO, 10%H_2O at 400°C).

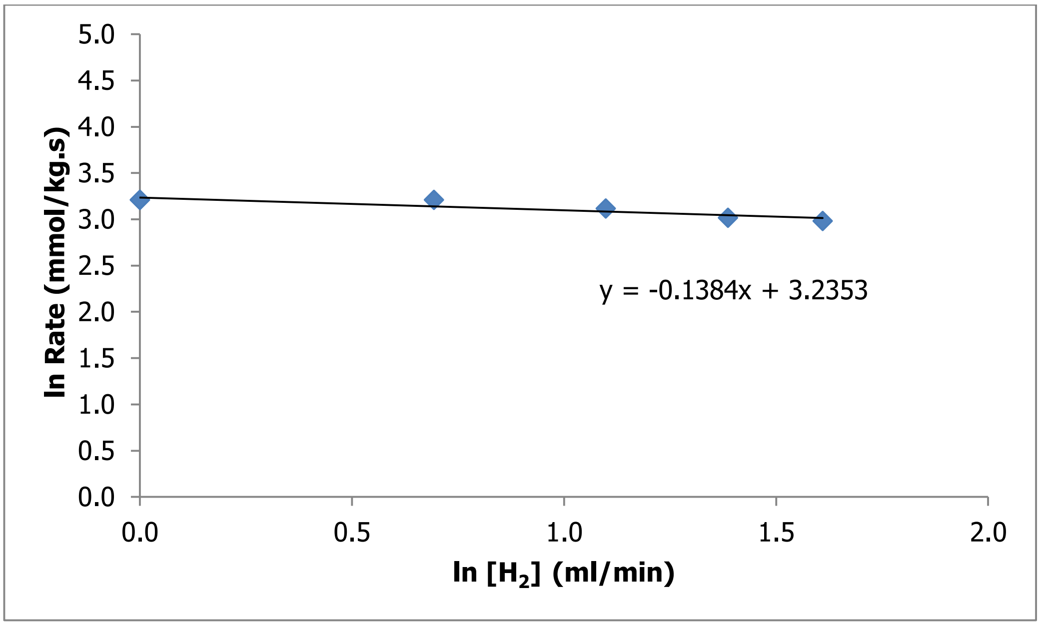

Figure 4.23 Reaction order of H_2 for 5%Ni/CeO_2 (using the inlet conditions of 1%CO, 1-5% H_2, 10%H_2O at 400°C).

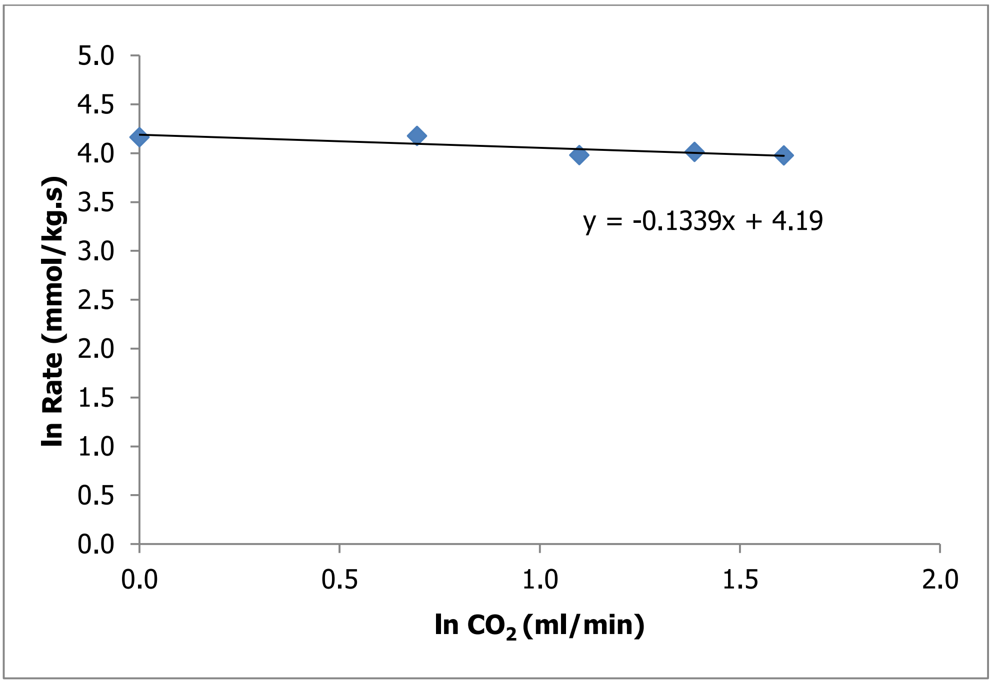

Figure 4.24 Reaction order of CO_2 for 5%Ni/CeO_2 (using the inlet conditions of 5%CO, 1-5% H_2, 10%H_2O at 400°C).

CHAPTER 5
CONCLUSIONS

In this study, the production of hydrogen via water gas shift reactions over several catalysts based on cerium oxide, including CeO_2, GDC and YDC was studied. Two different material preparation methods (i.e. precipitation and low temperature preparation) were compared. Furthermore, the effect of Ni impregnation to promote the reaction was also carried out. From XRD characterization, the fluorite type diffraction pattern of CeO_2 was observed in all samples. The Gd_2O_3 and Y_2O_3 peak identifications were not found in GDC and YDC indicating that Gd^{3+} and Y^{3+} readily incorporated into subsurface region of CeO_2 lattice to form solid solution. Addition of Ni did not cause any change in XRD patterns, presuming that Ni are highly dispersed on the surface of the supports. Nevertheless, an addition of Ni into doped ceria decreased the crystallite size and increased the catalyst surface area, according to BET study.

From the water gas shift activity test, it was found that the impregnation of Ni significantly promoted the catalyst activity. 5%Ni/20YDC showed the best activity among the catalysts prepared by low temperature method, from which the CO conversion started at the temperature above 250°C and reached 75% conversion at 350°C before declining at higher temperature. In case of catalysts prepared by co-precipitation method, 5%Ni/CeO_2 obtained the highest activity, from which the CO conversion reached 92% conversion at 400°C. The TPR was used to confirm the water gas shift activity. Good agreement between the TPR trends and catalyst activities was observed, from which the impregnation of Ni can lower the catalyst reducing temperature and the reaction can take place rapidly. Lastly, the activation energy and reaction orders of H_2, CO and CO_2 of 5%Ni/CeO_2 were predicted by the kinetics study. From the study, the activation energy (E_a) of 5%Ni/CeO_2 was 27 kJ/mol, while the reaction orders of H_2, CO and CO_2 were 0.69, -0.13 and -0.13, respectively. This indicates the weak negative effects of H_2 and CO_2 on the reaction due to the promotion of reverse water gas shift reaction by both compounds.

REFERENCES

[1]. Navarro, R., et al., *Hydrogen production from renewable sources: biomass and photocatalytic opportunities.* Energy & Environmental Science, 2009. **2**(1): p. 35-54.

[2]. Ebert, j. *syngastek*. 2011; Available from: http://syngastek.org/biocomposites/.

[3]. Francis, M., *Modeling: driving fuel cells.* Materials Today, 2002: p. 34-39.

[4]. Jason, H.G., Fuel cell technology, 2002.

[5]. Poggio-Fraccari, E., et al., *Copper and nickel catalysts supported on praseodymium-doped ceria (PDC) for the water-gas shift reaction.* Applied Catalysis A: General, 2013. **460–461**(0): p. 15-20.

[6]. Shantha, B.S.R.J.M.L.M.S., *A Review of the Water Gas Shift Reaction Kinetics.* International Journal of Chemical Reactor Engineering, 2010. **8**(1).

[7]. Newsome, D.S., *The Water-Gas Shift Reaction.* Catalysis Reviews: Science and Engineering, 1980. **21**(2): p. 275-318.

[8]. Callaghan, C., *Kinetics and Catalysis of the Water-Gas-Shift Reaction.* 2006.

[9]. Alchin, L., *The Element Hydrogen.* 2014.

[10]. *Hydrogen*. Available from: http://en.wikipedia.org/wiki/Hydrogen.

[11]. Education, T.J.N.A.F.-O.o.S., *The Element Hydrogen.* 2014.

[12]. Minh, N.Q. and T. Takahashi, *Chapter 1 - Introduction,* in *Science and Technology of Ceramic Fuel Cells,* N.Q. Minh and T. Takahashi, Editors. 1995, Elsevier Science Ltd: Oxford. p. 1-14.

[13]. Acres, G.J.K., et al., *Electrocatalysts for fuel cells.* Catalysis Today, 1997. **38**(4): p. 393-400.

[14]. Wongyao, N., *Hydrogen production and fuel cells technology.* 2005.

[15]. Xianguo, L., *Chapter 5: Alkaline fuel cells.* 2001.

[16]. *Fuel Cells*. 2014; Available from: http://www.fuelcells.org/.

[17]. Aguiar, P., et al., *Improving catalyst structures and reactor configurations for autothermal reaction systems: application to solid oxide fuel cells.* Chemical Engineering Science, 2001. **56**(2): p. 651-658.

[18]. education, B.s. *Hydrogen: the most common gas*. Available from: http://www.boconline.co.uk/hydrogen

[19]. Inc, M.A. *Hydrogen production methods*. 2014; Available from: http://www.mpr.com/pubs/hydroprod.pdf

[20]. Mattos, L.V., et al., *Partial oxidation of methane on Pt/Ce–ZrO2 catalysts.* Catalysis Today, 2002. **77**(3): p. 245-256.

[21]. Liu, Z.-W., et al., *Hydrogen production for fuel cells through methane reforming at low temperatures.* Journal of Power Sources, 2002. **111**(2): p. 283-287.

[22]. Igarashi, H., et al., *CO tolerance of Pt alloy electrocatalysts for polymer electrolyte fuel cells and the detoxification mechanism.* Physical Chemistry Chemical Physics, 2001. **3**(3): p. 306-314.

[23]. Trimm, D.L. and Z.I. Onsan, catalysis review, 2001. **43**: p. 31.

[24]. Q.Fu, et al., *Nanostructured Au-CeO2 water-gas shift catalysts.* Chem Eng, 2003. **93**: p. 41.

[25]. Le Page, J.F. *Applied heterogeneous catalysis design, manufacture, use of solid catalysts*. 1987; Available from: http://catalog.hathitrust.org/api/volumes/oclc/17615865.html.

[26]. Wilkindon, A.D.M.a.A. *catalyst*. 1997; Available from: http://www.iupac.org/goldbook/C00876.pdf.

[27]. Ertl, G., H. Knözinger, and J. Weitkamp, *Preparation of solid catalysts*. 2008: John Wiley & Sons.

[28]. Campanati, M., G. Fornasari, and A. Vaccari, *Fundamentals in the preparation of heterogeneous catalysts.* Catalysis Today, 2003. **77**(4): p. 299-314.

[29]. de Leitenburg, C., et al., *The effect of doping CeO2 with zirconium in the oxidation of isobutane.* Applied Catalysis A: General, 1996. **139**(1–2): p. 161-173.

[30]. Martinez-Arias, A., et al., Phys. Chem. B, 2000. **104**: p. 4038-4046.

[31]. Mamontov, E. and J. Soria, Phys. Chem. B, 2000. **104**: p. 11110-11116.

[32]. Steele, B.C.H., *Appraisal of Ce1−yGdyO2−y/2 electrolytes for IT-SOFC operation at 500°C.* Solid State Ionics, 2000. **129**(1–4): p. 95-110.

[33]. Kilner, J.A., *Fast oxygen transport in acceptor doped oxides.* Solid State Ionics, 2000. **129**(1–4): p. 13-23.

[34]. Knight, K.S., M. Soar, and N. Bonanos, *Crystal structures of gadolinium-and yttrium-doped barium cerate.* J. Mater. Chem., 1992. **2**(7): p. 709-712.

[35]. Montross, C.S., *Precipitation and bulk property behaviour in the yttria-magnesia-zirconia ternary system.* British ceramic. Transactions and journal, 1991. **90**(6): p. 175-178.

[36]. Song, X., et al., *Synthesis and Characterization of Y-Doped Mesoporous CeO2 Using A Chemical Precipitation Method.* Journal of Rare Earths, 2007. **25**(4): p. 428-433.

[37]. Ivanov, V.V., et al., *Conductivity and structure features of Ce1−xGdxO2−δ solid electrolytes fabricated by compaction and sintering of weakly agglomerated nanopowders.* Journal of the European Ceramic Society, 2007. **27**(2–3): p. 1041-1046.

[38]. Yu, T., et al., *Large-Scale Nonhydrolytic Sol–Gel Synthesis of Uniform-Sized Ceria Nanocrystals with Spherical, Wire, and Tadpole Shapes.* Angewandte Chemie International Edition, 2005. **44**(45): p. 7411-7414.

[39]. Chourashiya, M.G., et al., *Studies on structural, morphological and electrical properties of Ce1−xGdxO2−(x/2).* Materials Chemistry and Physics, 2008. **109**(1): p. 39-44.

[40]. Mahata, T., et al., *Combustion synthesis of gadolinia doped ceria powder.* Journal of Alloys and Compounds, 2005. **391**(1–2): p. 129-135.

[41]. Prasad, D.H., et al., *Synthesis of nano-crystalline Ce0.9Gd0.1O1.95 electrolyte by novel sol–gel thermolysis process for IT-SOFCs.* Journal of the European Ceramic Society, 2008. **28**(16): p. 3107-3112.

[42]. Fuentes, R.O. and R.T. Baker, *Structural, morphological and electrical properties of Gd0.1Ce0.9O1.95 prepared by a citrate complexation method.* Journal of Power Sources, 2009. **186**(2): p. 268-277.

[43]. Djinović, P., et al., *Comparison of water–gas shift reaction activity and long-term stability of nanostructured CuO-CeO2 catalysts prepared by hard template and co-precipitation methods.* Applied Catalysis A: General, 2009. **364**(1–2): p. 156-165.

[44]. Dikmen, S., et al., *Hydrothermal synthesis and properties of Ce1−xGdxO2−δ solid solutions.* Solid State Sciences, 2002. **4**(5): p. 585-590.

[45]. Augusto, B.L., et al., *Nickel/gadolinium-doped ceria anode for direct ethanol solid oxide fuel cell.* International Journal of Hydrogen Energy, 2014. **39**(21): p. 11196-11209.

[46]. Hennings, U. and R. Reimert, *Stability of rhodium catalysts supported on gadolinium doped ceria under steam reforming conditions.* Applied Catalysis A: General, 2008. **337**(1): p. 1-9.

[47]. Lin, J.-H., et al., *Hydrogen production by water–gas shift reaction over bimetallic Cu–Ni catalysts supported on La-doped mesoporous ceria.* Applied Catalysis A: General, 2010. **387**(1–2): p. 87-94.

[48]. Huang, S.-C., C.-H. Lin, and J.H. Wang, *Trends of Water Gas Shift Reaction on Close-Packed Transition Metal Surfaces.* The Journal of Physical Chemistry C, 2010. **114**(21): p. 9826-9834.

[49]. Huang, T.-J. and H.-M. Chen, *Hydrogen production via steam reforming of methanol over Cu/(Ce,Gd)O2−x catalysts.* International Journal of Hydrogen Energy, 2010. **35**(12): p. 6218-6226.

[50]. Chayakul, K., T. Srithanratana, and S. Hengrasmee, *Catalytic activities of Re–Ni/CeO2 bimetallic catalysts for water gas shift reaction.* Catalysis Today, 2011. **175**(1): p. 420-429.

[51]. Dohčević-Mitrović, Z.D., et al., *The size and strain effects on the Raman spectra of Ce1−xNdxO2−δ (0≤x≤0.25) nanopowders.* Solid State Communications, 2006. **137**(7): p. 387-390.

APPENDIXES

1) Crystallite size

Table A.1 Crystallite size of supports synthesized by low temperature method.

	@ 2-Theta	FWHM
CeO_2	28.502 (0.008)	0.641 (0.010)
10GDC	28.444 (0.013)	0.703 (0.016)
20GDC	28.355 (0.014)	0.683 (0.017)
10YDC	28.459 (0.010)	0.739 (0.012)
20YDC	28.432 (0.019)	1.003 (0.023)

Table A.2 Crystallite size of catalysts synthesized by low temperature method.

	@ 2-Theta	FWHM
5%Ni - CeO_2	28.548 (0.007)	0.567 (0.007)
5%Ni - 10GDC	28.497 (0.010)	0.577 (0.010)
5%Ni - 20GDC	28.463 (0.009)	0.498 (0.009)
5%Ni - 10YDC	28.574 (0.008)	0.583 (0.008)
5%Ni - 20YDC	28.554 (0.008)	0.504 (0.009)

Table A.3 Crystallite size of supports synthesized by co-precipitation method.

	@ 2-Theta	FWHM
CeO_2	28.503 (0.008)	0.635 (0.009)
10GDC	28.438 (0.013)	0.809 (0.013)
10YDC	28.526 (0.023)	1.043 (0.032)

Table A.4 Crystallite size of catalysts synthesized by co-precipitation method.

	@ 2-Theta	FWHM
5%Ni - CeO_2	28.527 (0.004)	0.318 (0.009)
5%Ni - 10GDC	28.474 (0.004)	0.338 (0.004)
5%Ni - 10YDC	28.525 (0.003)	0.318 (0.004)

2) Surface area

Table A.5 Surface area of supports synthesized by low temperature method.

	Area (m^2/g)	Slope	Y - Intercept
CeO_2	7.701E+01	4.502E+01	2.029E-01
10GDC	7.606E+01	4.528E+01	5.027E-01
20GDC	3.723E+01	9.256E+01	9.677E-01
10YDC	6.613E+01	5.206E+01	6.014E-01
20YDC	1.095E+02	3.143E+01	3.778E-01

Table A.6 Surface area of catalysts synthesized by low temperature method.

	Area (m²/g)	Slope	Y - Intercept
5%Ni - CeO_2	3.332E+01	1.032E+02	1.308E+00
5%Ni - 10GDC	4.914E+01	7.010E+01	7.647E-01
5%Ni - 20GDC	2.285E+01	1.504E+02	1.987E+00
5%Ni - 10YDC	4.486E+01	7.662E+01	1.016E+00
5%Ni - 20YDC	1.073E+01	3.242E+02	2.302E-01

Table A.7 Surface area of supports synthesized by co-precipitation method.

	Area (m²/g)	Slope	Y - Intercept
CeO_2	6.383E+01	5.390E+01	6.568E-01
10GDC	7.984E+01	4.315E+01	4.716E-01
10YDC	2.694E+01	1.286E+02	6.353E-01

Table A.8 Surface area of catalysts synthesized by co-precipitation method.

	Area (m²/g)	Slope	Y - Intercept
5%Ni - CeO_2	1.235E+01	2.817E+02	2.620E-01
5%Ni - 10GDC	1.432E+01	2.425E+02	6.695E-01
5%Ni - 10YDC	0.829E+01	2.035E+02	4.353E-01

3) GC Calibration

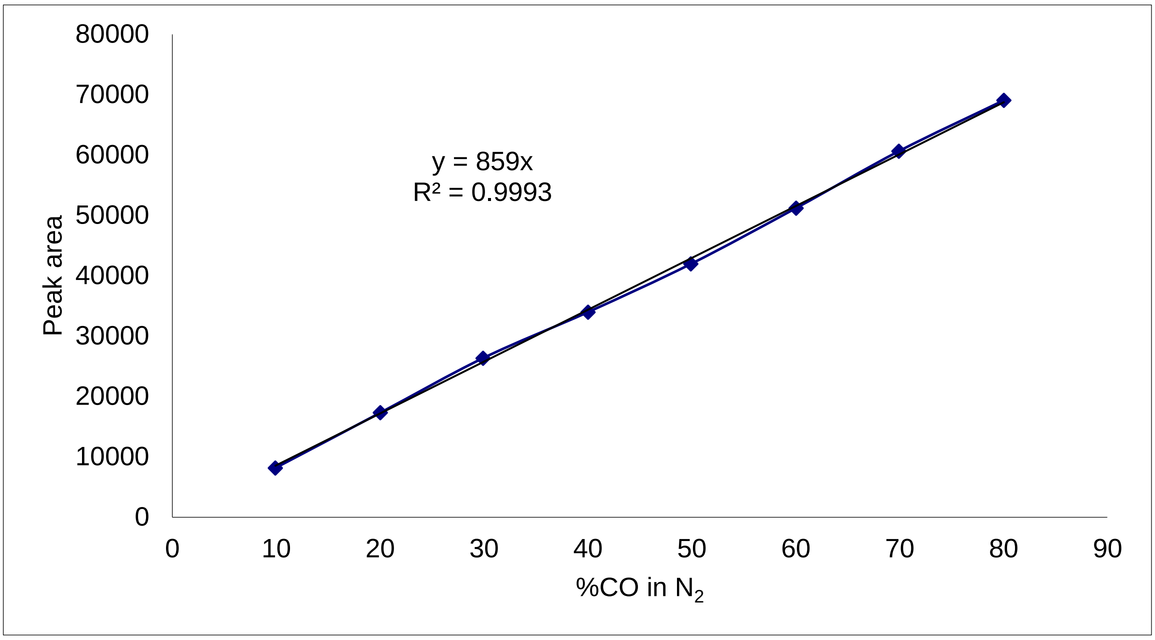

Figure A.1 GC Calibration curve of 15%CO in N_2

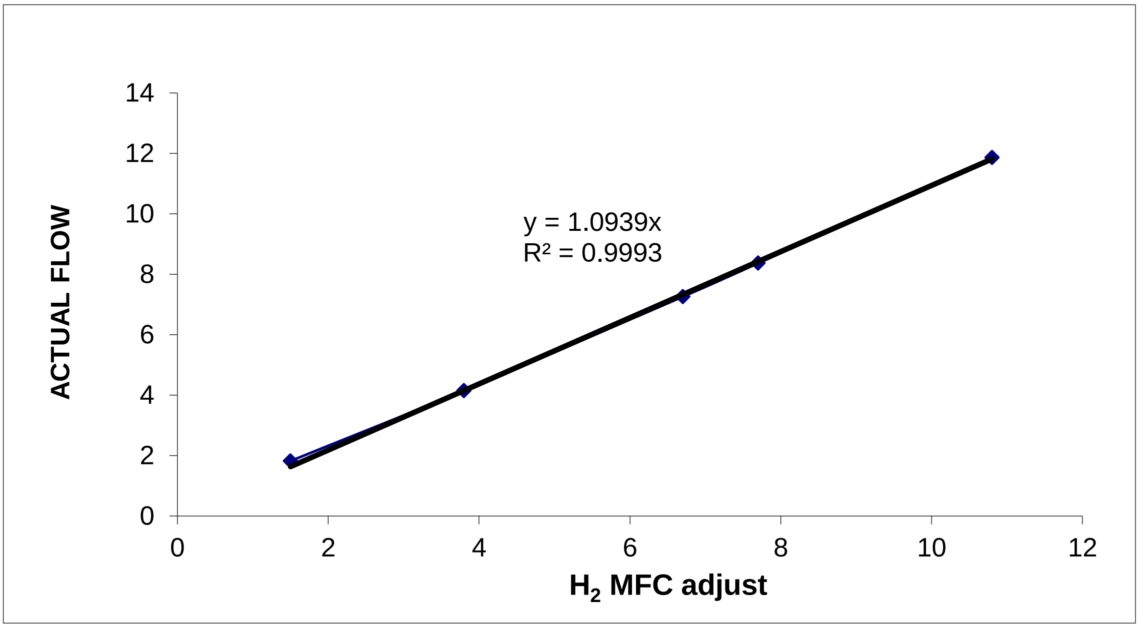

Figure A.2 MFC Calibration curve of H_2

Table A.9 Data of MFC setting for GC calibration

MFC setting for GC calibration			
X = MFC setting flow rate Y = actual flow rate	N_2 MFC : y = 1.0251x H_2 MFC : y = 1.0939x	x = y/1.0251 x = y/1.0939	
N_2		H_2	
Flow rate (%)	MFC setting	Flow rate (%)	MFC setting
99	96.5759438	1	0.91416034
98	95.6004292	2	1.82832069
96.035	93.6835431	3.965	3.62464576
96	93.6494001	4	3.65664137
94	91.6983709	6	5.48496206
92	89.7473417	8	7.31328275
90	87.7963126	10	9.14160344
88	85.8452834	12	10.9699241
86	83.8942542	14	12.7982448
84	81.9432251	16	14.6265655
82	79.9921959	18	16.4548862
81	79.0166813	19	17.3690465
90.1	87.8645986	9.93	9.07761221
85.1	83.0114135	14.91	13.6255599
75.2	73.3245537	24.84	22.7031721
65.5	63.8766950	34.52	31.5568151
55.1	53.7020778	44.95	41.0915075
45.9	44.7380743	54.14	49.4917268
35.7	34.8053848	64.32	58.7997075
25.0	24.3888401	75.00	68.5611116
66.6	64.9692713	33.40	30.5329555
33.2	32.3870842	66.80	61.065911
33.4	32.6251097	66.56	60.8428558
66.5	64.8424544	33.53	30.6517963
86.6	84.4688323	13.41	12.2598044
79.9	77.9280070	20.12	18.3892495
73.2	71.3871817	26.82	24.5186946
66.5	64.8424544	33.53	30.6517963
60.0	58.5474588	39.98	36.5508730
93.3	91.0096576	6.71	6.13035927